Journal of the American Heart Association

ORIGINAL RESEARCH

Reducing Morbidity and Mortality in Patients With Coarctation Requires Systematic Differentiation of Impacts of Mixed Valvular Disease on Coarctation Hemodynamics

Reza Sadeghi, PhD; Benjamin Tomka, BSc; Seyedvahid Khodaei, MASc; Julio Garcia, PhD; Javier Ganame, MD; Zahra Keshavarz-Motamed, PhD

BACKGROUND: Despite ongoing advances in surgical techniques for coarctation of the aorta (COA) repair, the long-term results are not always benign. Associated mixed valvular diseases (various combinations of aortic and mitral valvular pathologies) are responsible for considerable postoperative morbidity and mortality. We investigated the impact of COA and mixed valvular diseases on hemodynamics.

METHODS AND RESULTS: We developed a patient-specific computational framework. Our results demonstrate that mixed valvular diseases interact with COA fluid dynamics and contribute to speed up the progression of the disease by amplifying the irregular flow patterns downstream of COA (local) and exacerbating the left ventricular function (global) (N=26). Velocity downstream of COA with aortic regurgitation alone was increased, and the situation got worse when COA and aortic regurgitation coexisted with mitral regurgitation (COA with normal valves: 5.27 m/s, COA with only aortic regurgitation: 8.8 m/s, COA with aortic and mitral regurgitation: 9.36 m/s; patient 2). Workload in these patients was increased because of the presence of aortic stenosis alone, aortic regurgitation alone, mitral regurgitation alone, and when they coexisted (COA with normal valves: 1.0617 J; COA with only aortic stenosis: 1.225 J; COA with only aortic regurgitation: 1.6512 J; COA with only mitral regurgitation: 1.3599 J; patient 1).

CONCLUSIONS: Not only the severity of COA, but also the presence and the severity of mixed valvular disease should be considered in the evaluation of risks in patients. The results suggest that more aggressive surgical approaches may be required, because regularly chosen current surgical techniques may not be optimal for such patients.

Key Words: aortic fluid dynamics ■ coarctation ■ global hemodynamics ■ left ventricle metrics ■ local hemodynamics ■ mixed valvular disease

Coarctation of the aorta (COA) is one of the most common congenital heart defects, accounting for 5% to 8% of all congenital heart defects, occurring in ≈3 out of 10 000 of live births.[1–3] COA is often present in conjunction with other cardiac pathologies, mainly alongside mixed valvular diseases (MVDs).[4–7] MVDs are classified as various combinations of aortic and mitral valvular pathologies occurring simultaneously. COA is commonly associated with the bicuspid aortic valve, because up to 85% of patients with COA suffer from both pathologies.[1,4,8] Additionally, aortic stenosis (AS) and aortic regurgitation (AR) are commonly found alongside COA, occurring in 5% to 15% and 2% to 4% of cases, respectively.[9–14] Furthermore, COA is

Correspondence to: Zahra Keshavarz-Motamed, McMaster University, Department of Mechanical Engineering (Mail to JHE-310), Hamilton, Ontario, Canada, L8S 4L7. E-mail: motamedz@mcmaster.ca

For Sources of Funding and Disclosures, see page 24.

JAHA is available at: www.ahajournals.org/journal/jaha

CLINICAL PERSPECTIVE

What Is New?

- Doppler echocardiography pressure gradient across coarctation is a poor indicator to assess the disease severity when coexisting with mixed valvular disease (various combinations of aortic and mitral valvular pathologies).
- Catheter pressure gradient fails to reflect the effect of mixed valvular disease on the clinical assessment of coarctation hemodynamics.
- Mixed valvular disease exacerbates the coarctation hemodynamics (local) and contributes to speed up the progression of the disease by amplifying the irregular flow patterns downstream of coarctation. Mixed valvular disease exacerbated the left ventricular function and hemodynamics (global).

What Are the Clinical Implications?

- To assess risks in patient with coarctation of the aorta, not only the severity of coarctation, but also the presence and the severity of mixed valvular disease (various combinations of aortic and mitral valvular pathologies) should be considered.
- The results suggest that more aggressive surgical approaches may be required, because regularly chosen current surgical techniques may not be optimal for such patients.

Nonstandard Abbreviations and Acronyms

3D	3-dimensional
4D	4-dimensional
AR	aortic regurgitation
AS	aortic stenosis
COA	coarctation of the aorta
LBM	lattice Boltzmann method
MR	mitral regurgitation
MVD	mixed valvular disease
TAWSS	time-averaged wall shear stress

frequently found alongside mitral valve diseases, presenting itself in 20% to 59% of all patients with mitral pathologies.[15–17] The common mitral valve diseases found to coexist with COA include mitral stenosis (MS) and mitral regurgitation (MR), occurring in 3% and 2% to 5% of patients with COA, respectively.[18–24] COA and MVDs have significant effects on the left ventricle (LV), and if not treated promptly, are likely to result in LV dysfunction, cardiac failure, and death.[25–30]

Although COA is readily diagnosed, and interventional/surgical therapies are implemented, areas of contention and uncertainty remain. The coexistence of MVDs alongside COA poses many clinical challenges for diagnosis and assessment. A hemodynamically significant COA is often defined as a catheter pressure gradient or resting or exercise Doppler pressure gradient of 20 mmHg across the site of coarctation. Although most cardiologists agree that a pressure gradient >20 mmHg warns of severe COA and warrants interventional/surgical repair, it has yet to be determined whether MVD has any impact on the pressure gradient across the site of COA. The severity of COA may be masked by the hemodynamic effects of MVDs, and vice versa, ultimately resulting in clinical challenges for accurate diagnosis and assessment.[20,31–33] The optimal method and timing of intervention often remain unclear when MVDs are present, given the balance of risks for early and late mortality and reoperation.[22,34–37] Because of the complexity of treatment for COA and MVDs, there are increased rates of postoperative mortality.[15,38] Moreover, when COA and MVDs are present, surgery is often performed in a multistage approach, because higher morbidity rates have been recorded if multiple pathologies are repaired simultaneously.[22,36] Treatment strategies for patients with COA and MVDs are unclear and differ on an individualized basis, and some groups suggest that treatment strategies for patients with COA and MVDs may need to be redefined.[34,37] Before updating the current treatment recommendations, the quantitative understanding of the interplay between valvular pathologies and COA, and the breakdown of effects of each disease constituent on the cardiac function of the cardiovascular system is crucial.[39–41]

Cardiology is flow,[42] and therefore the essential sources of cardiovascular mortality and morbidity can be explained on the basis of adverse hemodynamics: abnormal biomechanical forces and flow patterns, leading to the development and progression of cardiovascular disease.[8,43–48] Precise and effective diagnosis hinges on the quantification of the following requirements: global hemodynamics: (1) metrics of cardiac function (eg, heart workload) and its contribution breakdown of each component of the cardiovascular diseases and of the local hemodynamics and (2) aortic fluid dynamics (eg, details of the instantaneous [3-dimensional] 3D flow). In this study, we developed a patient-specific, imaged-based computational-mechanics framework that dynamically couples the local hemodynamics with the global circulatory cardiovascular system using the 3D lattice Boltzmann method (LBM) and lumped parameter modeling to investigate the impact of COA and MVDs on both local and global hemodynamics (Figure 1) in 26 patients. The developed computational framework was validated against clinical cardiac catheterization data, Doppler echocardiography, and 4-dimensional (4D) flow magnetic resonance imaging (MRI) (Figures 2 and 3). To the best of

our knowledge, this is the first study that investigated the effects of MVDs on COA in terms of both local and global hemodynamics (Figures 4 through 14).

METHODS

Data Availability

The development and validation of the proposed method require the retrospective clinical data routinely measured in clinics (Doppler ultrasound and catheter data), which were transferred as the deidentified and anonymized data. The code and the optimization algorithms are available from the author upon request.

Study Population

Thirty-six deidentified and anonymous patients with COA and MVDs (see Table for patients' characteristics) between 2008 and 2019 at Stephenson Cardiac Imaging Centre, Libin Cardiovascular Institute of Alberta (Calgary, AB, Canada), and St. Joseph's Healthcare (Hamilton, ON, Canada) were considered. Informed consent was obtained from all participants. The selections were done by operators blinded to the objectives and contents of this study at each institution, and the protocols were reviewed and approved by the institutional review boards of each institution. All methods and measurements were performed in accordance with relevant guidelines and regulations, including guidelines of the American College of Cardiology and American Heart Association. Senior cardiologists reviewed the echocardiograms and reports using OsiriX imaging software (version 8.0.2; Pixmeo, Switzerland). Cardiac catheterization was performed to determine the pressure gradient and exact morphology of the COA in all patients. Computed tomography data were collected, including images and documented reports. Computed tomography images were segmented, and the 3D geometries of the complete aorta were reconstructed to be used for our computational model.

Numerical Study

We developed a computational fluid dynamics framework using the 3D LBM (large eddy simulation, Smagorinsky subgrid scale model) and lumped parameter modeling to simulate both the local and global hemodynamics in patients with MVDs and COA (Figure 1A, schematic diagram).

Global Hemodynamics (Cardiac Function Metrics and Hemodynamics)

Our developed patient-specific, Doppler-based lumped-parameter algorithm includes several submodels, allowing for the analysis of complex coarctation disease, for example, when COA coexists with the other valvular, vascular, and ventricular disease: (1) left atrium, (2) LV, (3) aortic valve, (4) mitral valve, (5) coarctation of the aorta, (6) systemic circulation, and (7) pulmonary circulation (Figure 1). Our Doppler-based lumped parameter algorithm uses the following input parameters that all can be reliably measured using Doppler echocardiography: forward left ventricular outflow tract stroke volume, heart rate, ejection time, ascending aorta area, left ventricular outflow tract area, aortic valve effective orifice area, mitral valve effective orifice area, COA severity, and grading of aortic and mitral valves regurgitation severity. Note that the proposed method does not need catheter data or any invasive data for estimating the cardiac function metrics (eg, workload). Other input parameters of the lumped parameter algorithm include systolic and diastolic blood pressures measured using sphygmomanometers. The calculations of the lumped parameter model were validated against cardiac catheterization data (the instantaneous pressures in the aorta and LV) in patients with complex valvular, ventricular, and vascular diseases with a wide range of cardiovascular diseases.[45,49]

Local Hemodynamics (3D Blood Flow Dynamics)

We developed a computational fluid dynamics framework to simulate the local hemodynamics in patients with COA in pre- and postintervention states (Figure 1). This framework is based on lumped parameter modeling[45,49] and 3D LBM (Smagorinsky subgrid scale model) as implemented in the open-source OpenLB library with some supplements as explained in Sadeghi et al.[44] Reynolds-averaged Navier-Stokes equations are common to model blood low; however, there are limitations to model pulsatile flows.[50] Direct numerical simulations put a burden on computing resources and are limited to low Reynolds numbers. Large eddy simulation, which falls between direct numerical simulations and Reynolds-averaged Navier-Stokes, is well suited for computational modeling of turbulent vascular flows, with great potential in modeling the physiological low-Reynolds pulsatile flows.[45] We used a 3D LBM-based computational fluid dynamics approach using large eddy simulation (Smagorinsky subgrid scale model) to simulate blood flow through the vascular system.[44] Calculations of this computational fluid dynamics framework were validated against 4D flow MRI measurements (Figures 2 and 3).

Model Properties and Boundary Conditions

Aortic local flow dynamics are greatly influenced by upstream and downstream flow conditions that must be accounted for. Additionally, the proper choice of

boundary conditions is critical, because they influence the accuracy of flow simulations. Blood was assumed to be a Newtonian and incompressible fluid with dynamic viscosity of 0.0035 Pa.s and density of 1050 kg/m^3. A lumped parameter model (Figure 1) simulated the function of the left side of the heart in the presence of COA and MVDs and was used to impose the time-dependent inlet flow at the ascending aorta cross section and the outlet pressure at the descending aorta cross section. The time-dependent flow rate obtained from the lumped parameter model was used to scale this profile to observe this time-varying inlet boundary condition (Figure 1). The inlet velocity boundary condition in the LBM was implemented using the method suggested by Skordos,[51] which uses a second-order finite difference scheme to compute the velocity gradient of the boundary nodes and extrapolates the pressure distribution at the inlet from bulk nodes.[52] Furthermore, a sinusoidal smooth start-up phase was used to begin the simulation and smoothly increase the initial condition for the velocity from 0 to avoid pressure fluctuation artifacts at the inlet.[53,54] The total flow rate headed to the branches was calculated using the lumped parameter model and then distributed to the branches based on the relative cross-sectional area of each branch. A no-slip boundary condition was applied at the solid walls as described above. Patients with COA are typically hypertensive and characterized by reduced compliance and elevated stiffness in both the proximal and distal aorta. Jin et al[55] and Keshavarz-Motamed et al[8,45,56] showed that a rigid-wall assumption for the aorta is acceptable, and thus, the aortic wall in this study was treated as such.

Because of the complex multiphysics nature of the aorta and the valves, the overall estimation of cardiac parameters is reliant on the outputs of the lumped-parameter algorithm that are in turn dependent on input parameters used in the lumped-parameter algorithm. Our patient-specific, Doppler-based lumped-parameter algorithm, which provided boundary conditions, was validated against clinical catheterization data in patients with a wide range of cardiovascular diseases.[44,45,49] We used the validated lumped-parameter algorithm[44,45,49] to obtain the boundary conditions. Moreover, our performed sensitivity analysis revealed negligible effects of changes (±20%) in the free parameters on the model output variables.[57]

Reconstructed Geometries in Patients With Coarctation

3D geometries of the complete aorta including ascending aorta, aortic branches, and descending aorta were reconstructed from segmented computed tomography images of patients using ITK-SNAP (version 3.8.0-BETA) (Figure 1). We used a smoothing procedure for the surfaces to overcome the challenges of computational convergence and stability. Change in the volume because of smoothing was <1% in all patients.

Numerical Strategy

Multiple and single relaxation time LBM-based models were coupled with Smagorinsky's turbulent model to stabilize complex turbulent fluid flow across the domain. For treating complex geometry, we used the second order accuracy method proposed by Bouzidi et al.[58] A smooth start-up phase was added to the inlet velocity condition to suppress the undesired pressure fluctuation. For turbulent modeling, a large eddy Smagorinsky subgrid-scale model with constant C_s=0.1 was applied.[59] Mesh sensitivity analysis was performed for maximum velocity and pressure drop at the coarctation region. Mesh definition was considered acceptable if no significant differences (lower than 5%) existed between successive mesh refinements in both quantities. The physical time step in this study was as low as 1.5 μs, and physical lattice height adjacent to the wall was as low as 50 μm to ensure that it is within the viscous sublayer.

4D Flow MRI

4D flow MRI is a recent development of phase-contrast MRI, with the capability of comprehensive blood flow assessment in 3 spatial dimensions over the cardiac cycle.[60] 4D flow MRI provides visualization of the vascular territory of interest and allows for the estimation of

Figure 1. Reconstructed geometry and simulation domain.
A, In this study, we developed a patient-specific, imaged-based computational-mechanics framework that dynamically couples the local hemodynamics with the global circulatory cardiovascular system to investigate the impact of the coarctation of the aorta and mixed valvular diseases on both local and global hemodynamics in these patients. We used computed tomography images from patients to segment and reconstruct the 3-dimensional (3D) geometries of the complete aorta. These 3D geometries were used for investigating hemodynamics using computational fluid dynamics. Local flow dynamics are greatly influenced by upstream and downstream flow conditions that are absent in the flow simulation domain. A patient-specific, Doppler-based lumped-parameter algorithm, described in details elsewhere,[49] simulated the function of the left side of the heart. Time-dependent inlet flow at the ascending aorta and outlet pressure at the descending aorta positions were obtained from our developed lumped parameter algorithm[49] and applied as boundary conditions. Boundary conditions of the aortic branches were adjusted to match the flow distribution. **B**, We compared 4-dimensional (4D) flow magnetic resonance imaging (MRI) data and results of our computational framework. The 3D geometry of the complete aorta was reconstructed using MRI images, and the entire volume of downsampled lattice Boltzmann model (LBM) data were smoothed[53,54] (see the 4D Flow MRI section in the text for more details). LV indicates left ventricle.

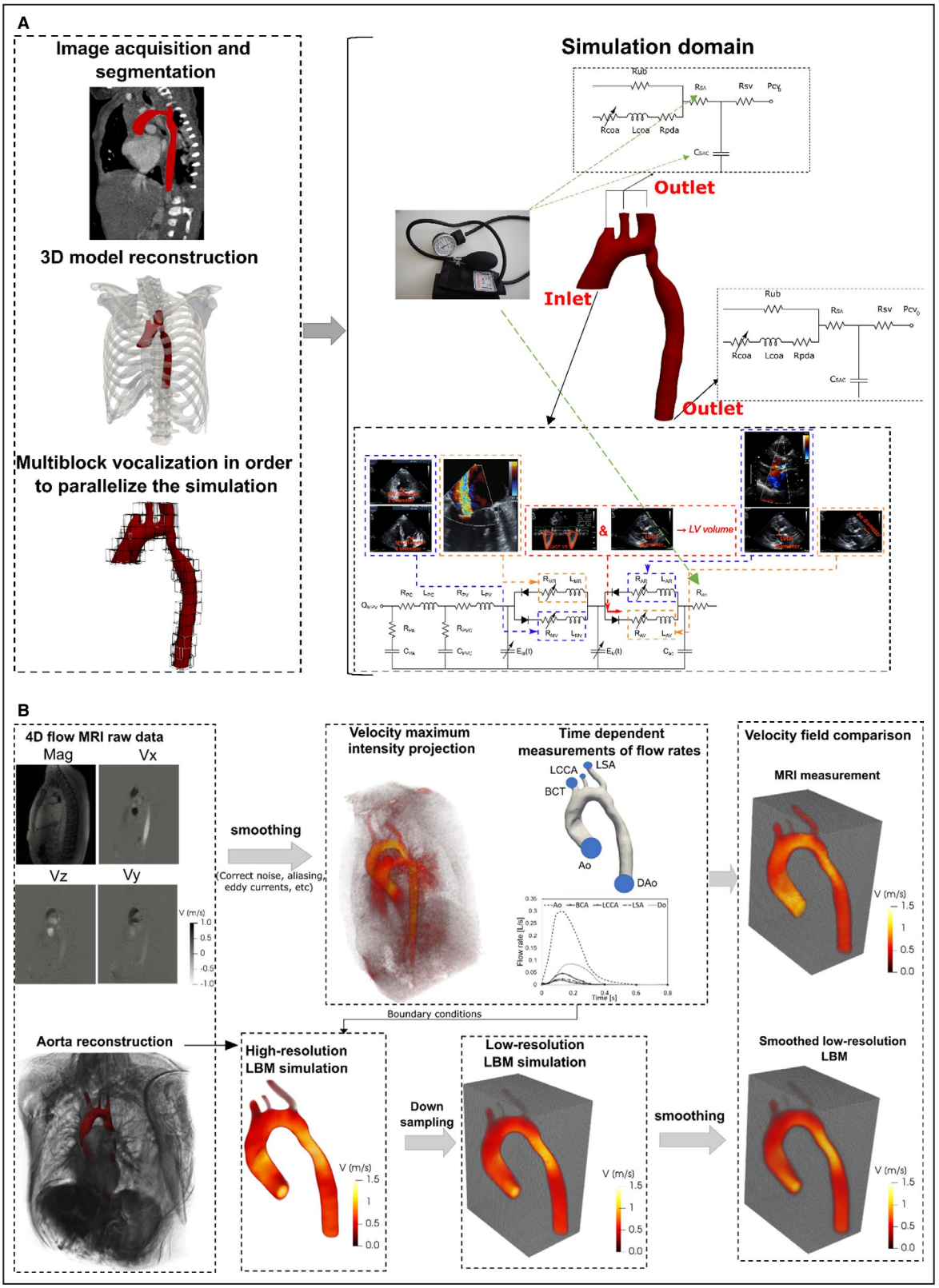

hemodynamic biomarkers such as wall shear forces[61] and pressure gradients.[62,63] Additionally, 4D flow MRI provides comprehensive information on complex flow patterns in vascular diseases.[64] In this study, acquisition of 4D flow MRI data in patients with COA and valvular diseases was performed (Figure 1B, data acquisition and analysis workflow of 4D flow MRI) by standard Cartesian 4D flow sequence using 1.5 T MRI

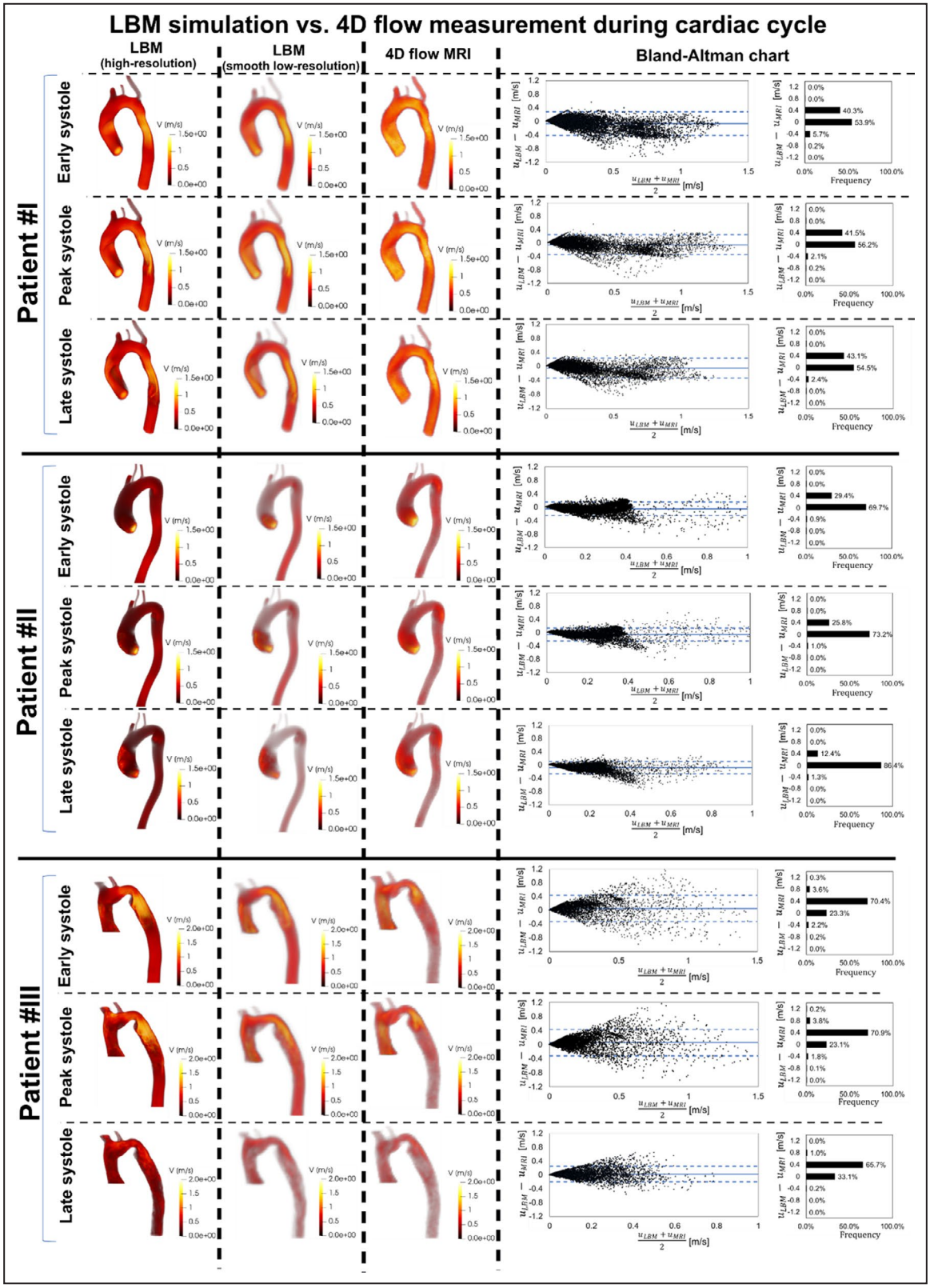

Figure 2. Validation against 4D flow MRI (part I).
We compared 4D flow MRI data and the results of the computational framework (based on the lumped parameter model and lattice Boltzmann model [LBM]) in sample patients I to III, qualitatively (revealed in velocity mapping) and quantitatively, by performing Pearson product moment correlation analysis on the entire domain during the cardiac cycle between smooth downsampled LBM and 4D flow MRI measurements. 4D indicates 4-dimensional; and MRI, magnetic resonance imaging.

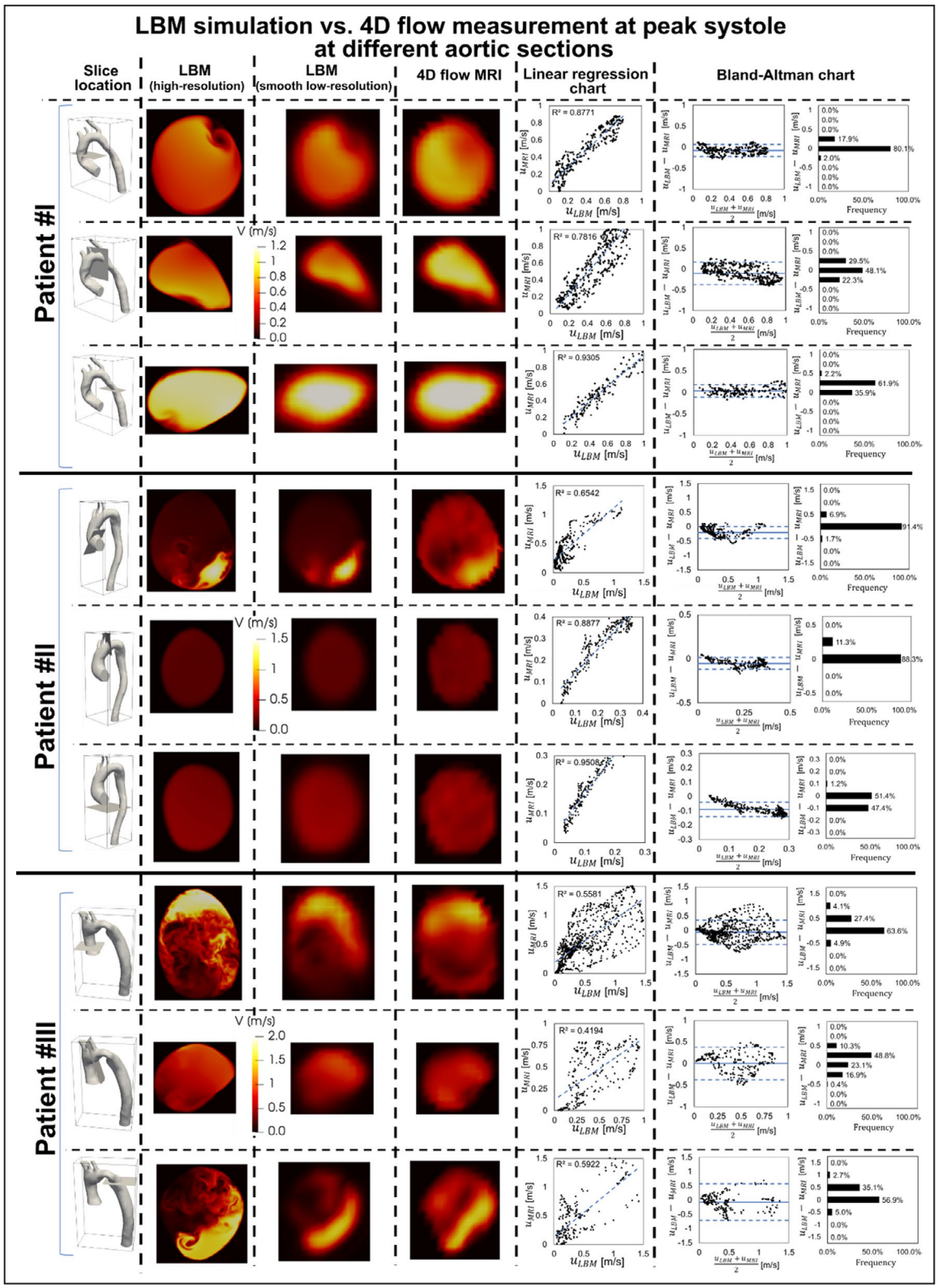

Figure 3. Validation against 4D flow MRI (part II).
We compared 4D flow MRI data and results of the computational framework (based on lumped parameter model and lattice Boltzmann model [LBM]) in sample patients I to III, qualitatively (revealed in velocity mapping) and quantitatively, by performing linear regression and Pearson product moment correlation analysis at different sections at peak systole between smooth downsampled LBM and PC-MRI measurements. 4D indicates 4-dimensional; MRI, magnetic resonance imaging; and PC, phase-contrast.

scanners (Philips Achieva; Philips Medical Systems, Best, the Netherlands). ECG gating synchronized and diaphragm navigator gated 4D flow MRI were performed during free breathing. Acquisition parameters were as follows: spatial resolution of 1.97 to 2.62, 1.97 to 2.62, 2.5 to 4 mm^3, temporal resolution of 36 to 40 ms. Velocity encoding was set to the range (1.5–4.5 m/s), and the total scan time for each measurement

Figure 4. Flow modeling (local) in patient 1.
Computed velocity magnitude and time-averaged wall shear stress (TAWSS) using the computational framework (lattice Boltzmann method and lumped parameter model) in sample patient 1. Actual patient (in red font in this figure) has severe aortic stenosis (EOA_{AS}=1 cm^2), moderate aortic valve regurgitation (EOA_{AR}=0.15 cm^2), moderate mitral valve regurgitation (EOA_{MR}=0.15 cm^2) with no mitral stenosis. This patient has brachial pressures of 70 and 125 mmHg, forward left ventricle (LV) stroke volume of 110 mL, maximum LV pressure of 170 mmHg, and LV workload of 2.4923 J. The total shear stress exerted on the wall throughout the cardiac cycle was evaluated using the TAWSS, which is obtained as $\text{TAWSS} = \frac{1}{T}\int_0^T |\tau|\, dt$. Here, T and τ are the cardiac cycle period and instantaneous wall shear stress, respectively. AR indicates aortic regurgitation; AS, aortic stenosis; EOA, effective orifice area; MR, mitral regurgitation; and MS, mitral stenosis.

varied from 8 to 15 minutes. All 4D flow data were corrected for multiple sources of phase offset errors and noises such as velocity aliasing, Maxwell terms, and eddy currents using an in-house MATLAB-based code (MathWorks). A data-smoothing algorithm proposed by Garcia[65,66] was used to eliminate random errors of the velocity vectors. Garcia[65,66] proposed a fully automated smoothing procedure based on a penalized least squares approach that allows fast smoothing of the data and can replace spurious or missing vector with the smoothed one.

The 3D segmentation of the thoracic aorta geometry and orifice shape of aortic stenosis or bicuspid valve was performed by ITK-SNAP (Yushkevich et al; http://www.itksnap.org) and an in-house MATLAB-based code. Fusion 3D (Autodesk) and Meshmixer (Autodesk) were used to smooth the geometry and fix the defects. Finally, the stereolithography format of the geometry (domain) was extracted for our computational simulation. Time-varying flow velocity information extracted from patient-specific 4D flow MRI data was imposed at the inlet and outlets of each LBM computational model. To study the effect of resolution and compare LBM to 4D flow MRI velocity fields on identical grids, we downsampled the high-resolution LBM velocities into phase-contrast MRI resolution by linear interpolation of LBM velocity on the MRI subgrid. Moreover, downsampled LBM data were subjected to an imitation of the smoothing inherent in the 4D flow MRI measurement to have the closest LBM approximation to the 4D flow MRI data. The downsampling and smoothing procedures are schematically shown in Figure 1B.

Velocity field extracted from 4D flow MRI measurements was smoothed through a multidimensional spline smoothing technique proposed by Garcia.[65,66] The algorithm deals with occurrences of missing and outlying values and eliminates random errors automatically. The mathematics behind algorithm structure is based on a penalized least squares approach that allows fast smoothing of the data and can replace a spurious or missing vector with the smoothed one. The algorithm allows fast unsupervised smoothing that combines the use of the discrete cosine transform and the generalized cross-validation score. Garcia's algorithm was compared with conventional methods, including the normalized median test and experimental raw particle image velocimetry velocity fields, and it was shown that it can easily deal with a large amount of missing data and reduce the experimental noise while keeping the most important characteristics of a data set.[65]

Table. Baseline Patient Characteristics

Characteristic	Preintervention value, n=36
Ventricular indices, DE findings	
Ejection fraction, %, mean±SD	59.5±11.5
Heart rate, bpm, mean±SD	65.8±10.6
Stroke volume, mL, mean±SD	62.3±10.4
NYHA classifications ≥ grade 2, %	39%
Valvular indices, DE findings	
Mean aortic valve gradient, mmHg, mean±SD	26±7.3
Maximum aortic valve gradient, mmHg, mean±SD	46±19.5
Aortic valve disease type, n	Tricuspid: 22, bicuspid: 14
Aortic valve regurgitation ≥ grade 2, %	36%
Mitral valve regurgitation ≥ grade 2, %	21%
Vascular indices, sphygmomanometer	
Brachial systolic blood pressure, mmHg, mean±SD	145±25.4
Brachial diastolic blood pressure, mmHg, mean±SD	78±11.9
Patient description	
Mean age, y, mean±SD (sex, %)	34±11.5 (women, 42%)
Mean weight, kg; mean height, cm, mean±SD	78±14.6; 169.3±7.9
Body surface area, m^2, mean±SD	1.8±0.31
Associated cardiovascular lesions, n	
Bicuspid aortic valve	14
Tricuspid aortic valve stenosis	6
Aortic valve regurgitation	12
Mitral valve stenosis	4
Heart failure	11
Mitral valve regurgitation	10
Descending aorta aneurysms	5

DE indicates Doppler echocardiography; and NYHA, New York Heart Association.

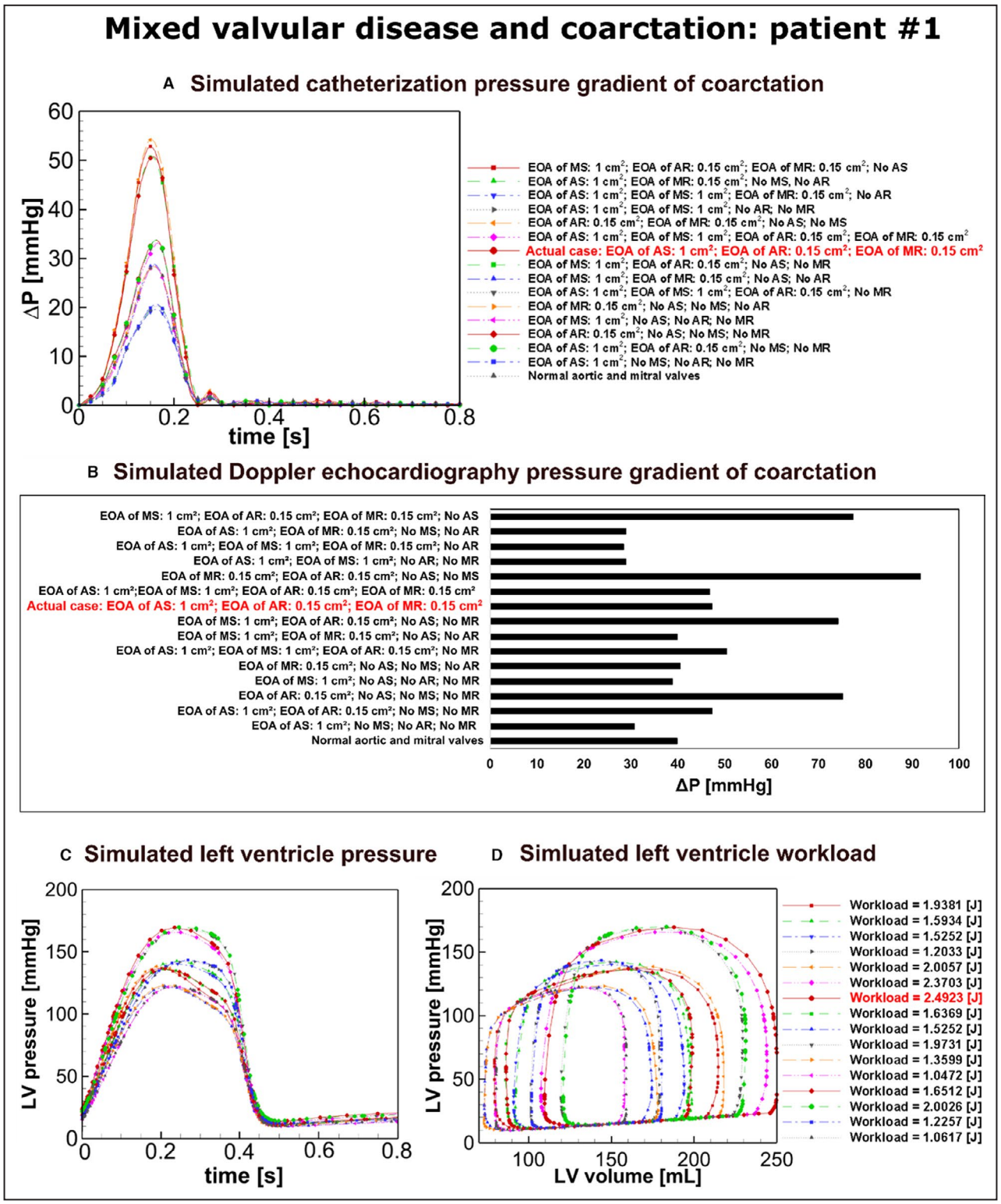

Figure 5. Flow modeling (global) in patient 1.

A, Simulated catheter pressure gradient of coarctation, which is the difference between the tabulated pressures of the neck and upstream of coarctation of the aorta (COA), using the computational framework, lattice Boltzmann method, and lumped parameter model ($\Delta P=P_2-P_1$; P_2: pressure at the neck of COA; P_1: pressure upstream of COA). **B**, Simulated peak Doppler echocardiography pressure gradient of coarctation using the computational framework, lattice Boltzmann method, and lumped parameter model ($\Delta P=4V_{max}^2$; V_{max}: maximum velocity downstream of COA during systole). **C**, Simulated LV pressure using lumped parameter model. **D**, Simulated LV workload using lumped parameter model. AR indicates aortic regurgitation; AS, aortic stenosis; EOA, effective orifice area; LV, left ventricle; MR, mitral regurgitation; and MS, mitral stenosis.

Figure 6. Flow modeling (local) in patient 2.
Computed velocity magnitude and time-averaged wall shear stress (TAWSS) using the computational framework (lattice Boltzmann method and lumped parameter model) in sample patient 1. Actual patient (in red font in this figure) has moderate aortic stenosis (EOA_{AS}=1.2 cm^2), moderate aortic valve regurgitation (EOA_{AR}=0.2 cm^2), with no mitral valve regurgitation and no mitral stenosis. This patient has brachial pressures of 60 and 131 mmHg, forward LV stroke volume of 124 mL, maximum LV pressure of 156.5 mmHg, and LV workload of 2.022 J. AR indicates aortic regurgitation; AS, aortic stenosis; EOA, effective orifice area; LV, left ventricle; MR, mitral regurgitation; and MS, mitral stenosis.

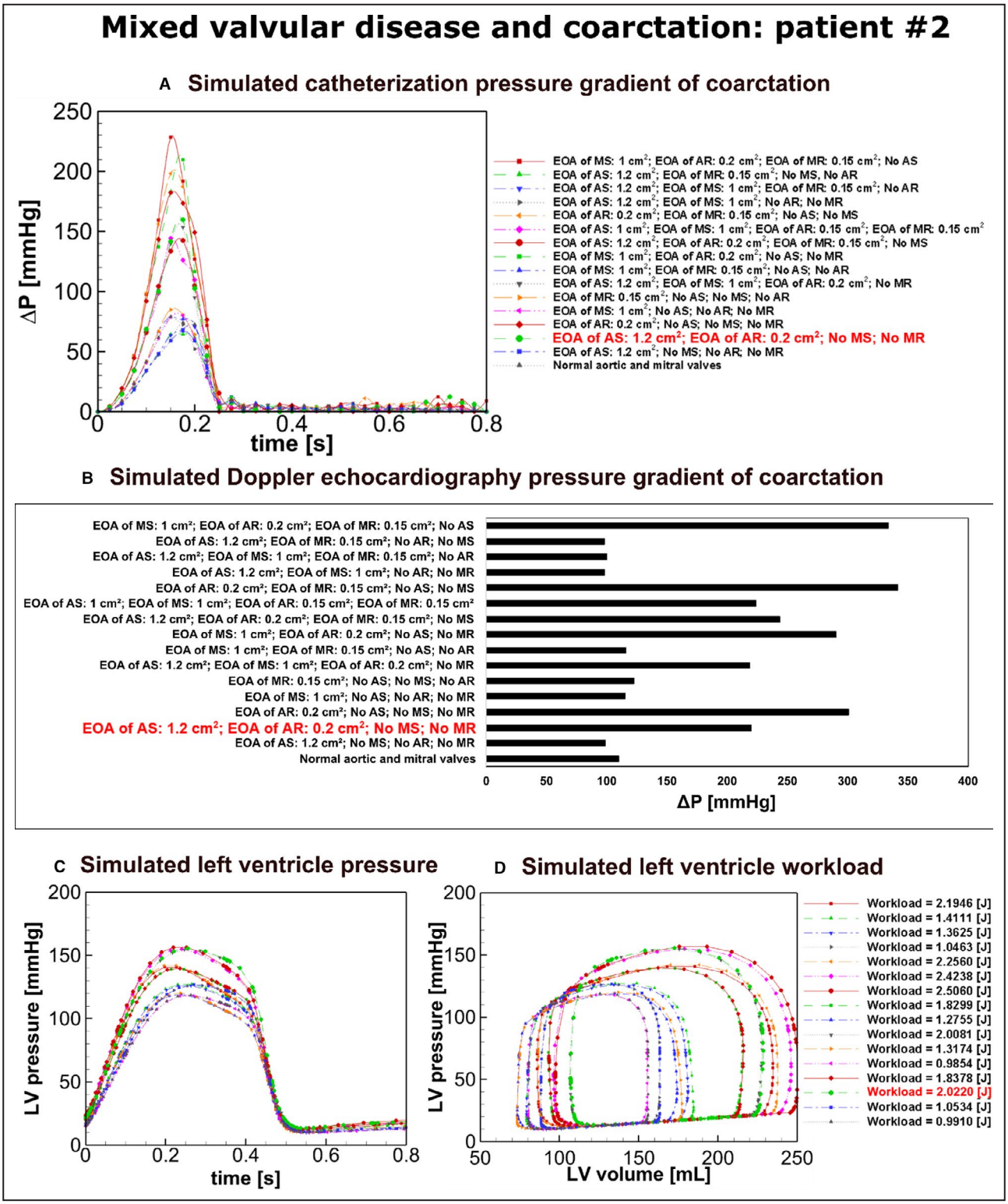

Figure 7. Flow modeling (global) in patient 2.
A, Simulated catheter pressure gradient of coarctation, which is the difference between the tabulated pressures of the neck and upstream of coarctation of the aorta (COA), using the computational framework, lattice Boltzmann method, and lumped parameter model ($\Delta P=P_2-P_1$; P_2: pressure at the neck of COA; P_1: pressure upstream of COA); **B**, Simulated peak Doppler echocardiography pressure gradient of coarctation using the computational framework, lattice Boltzmann method, and lumped parameter model ($\Delta P=4V_{max}^2$; V_{max}: maximum velocity downstream of COA during systole). **C**, Simulated LV pressure using lumped parameter model. **D**, Simulated LV workload using lumped parameter model. AR indicates aortic regurgitation; AS, aortic stenosis; EOA, effective orifice area; LV, left ventricle; MR, mitral regurgitation; and MS, mitral stenosis.

Figure 8. Flow modeling (local) in patient 3.
Computed velocity magnitude and time-averaged wall shear stress (TAWSS) using the computational framework (lattice Boltzmann method and lumped parameter model) in sample patient 1. Actual patient (in red font in this figure) has severe mitral stenosis (EOA_{MS}=1 cm^2), moderate aortic valve regurgitation (EOA_{AR}=0.2 cm^2), moderate mitral valve regurgitation (EOA_{AR}=0.15 cm^2), and no aortic stenosis. This patient has brachial pressures of 55 and 138 mmHg, forward LV stroke volume of 121 mL, maximum LV pressure of 142 mmHg, and LV workload of 2.2599. AR indicates aortic regurgitation; AS, aortic stenosis; EOA, effective orifice area; LV, left ventricle; MR, mitral regurgitation; and MS, mitral stenosis.

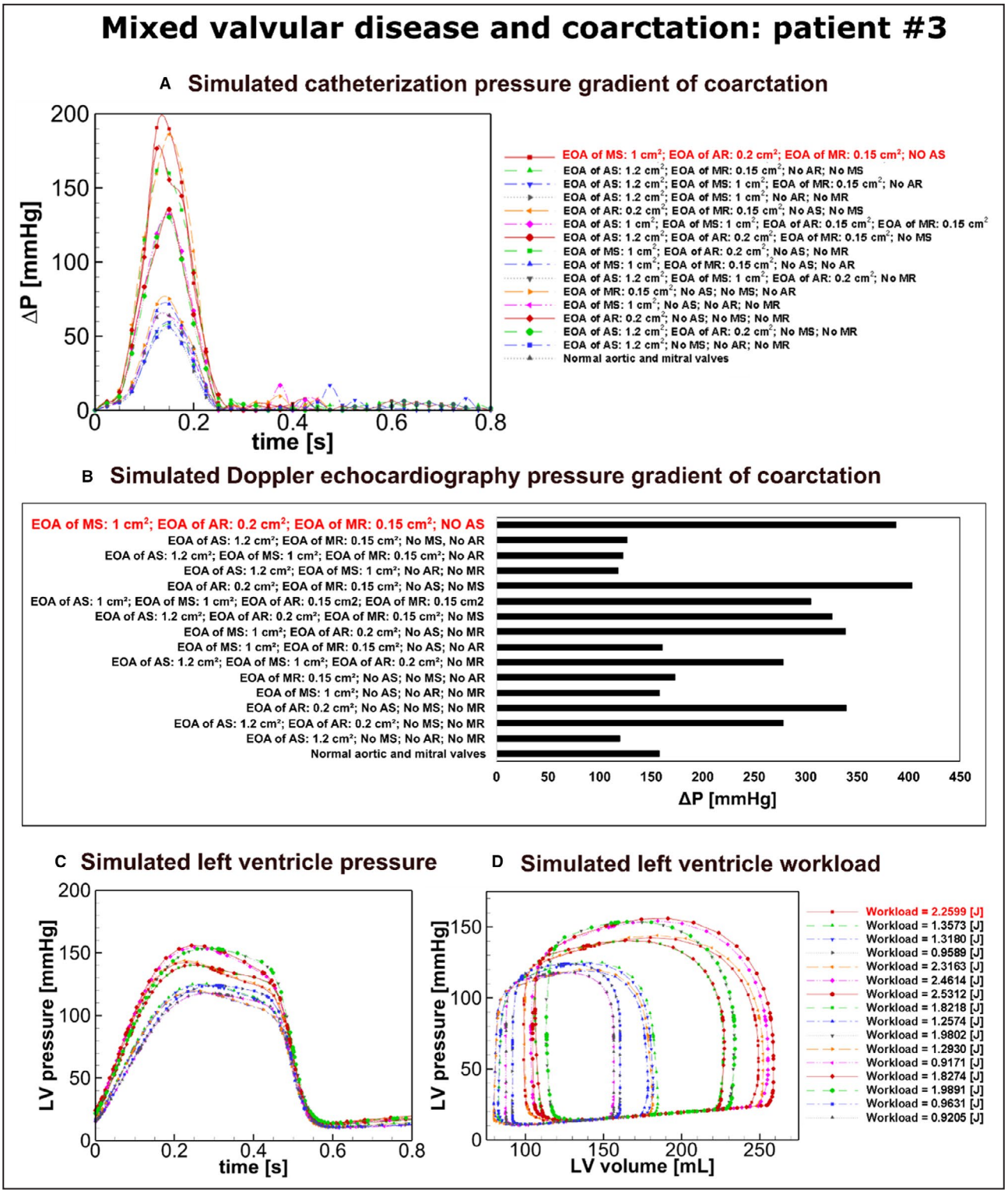

Figure 9. Flow modeling (global) in patient 3.

A, Simulated catheter pressure gradient of coarctation, which is the difference between the tabulated pressures of the neck and upstream of coarctation of the aorta (COA), using the computational framework, lattice Boltzmann method, and lumped parameter model ($\Delta P=P_2-P_1$; P_2: pressure at the neck of COA; P_1: pressure upstream of COA). **B**, Simulated peak Doppler echocardiography pressure gradient of coarctation using the computational framework, lattice Boltzmann method, and lumped parameter model ($\Delta P=4V_{max}^2$; V_{max}: maximum velocity downstream of COA during systole). **C**, Simulated LV pressure using lumped parameter model. **D**, Simulated LV workload using lumped parameter model. AR indicates aortic regurgitation; AS, aortic stenosis; EOA, effective orifice area; LV, left ventricle; MR, mitral regurgitation; and MS, mitral stenosis.

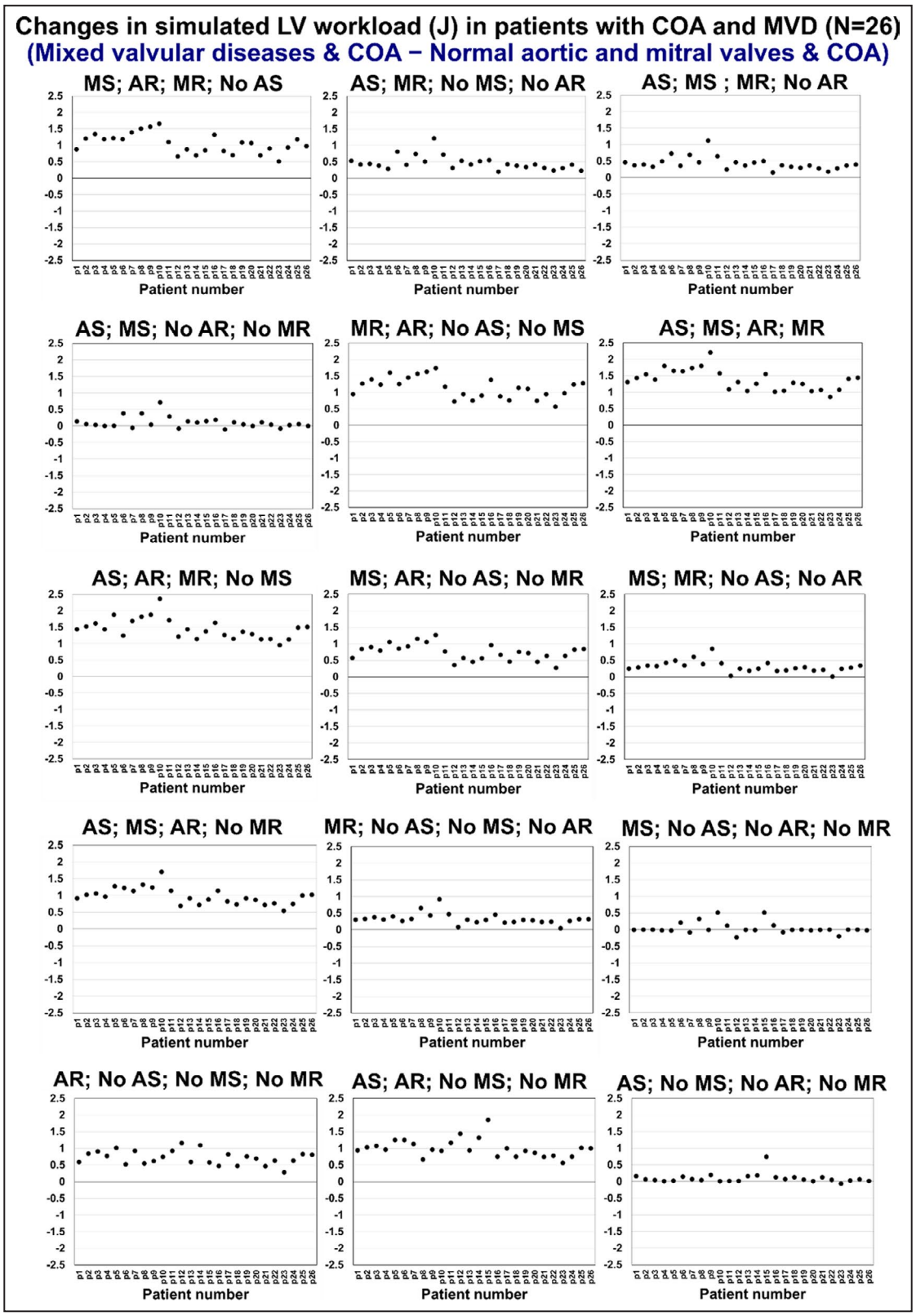

Figure 10. Differences in the simulated LV workloads between mixed valvular disease, and COA and normal aortic and mitral valves and COA, in individual patients (N=26).

AR indicates aortic regurgitation; AS, aortic stenosis; COA, coarctation of the aorta; LV, left ventricle; MR, mitral regurgitation; MS, mitral stenosis; and MVD, mixed valvular disease.

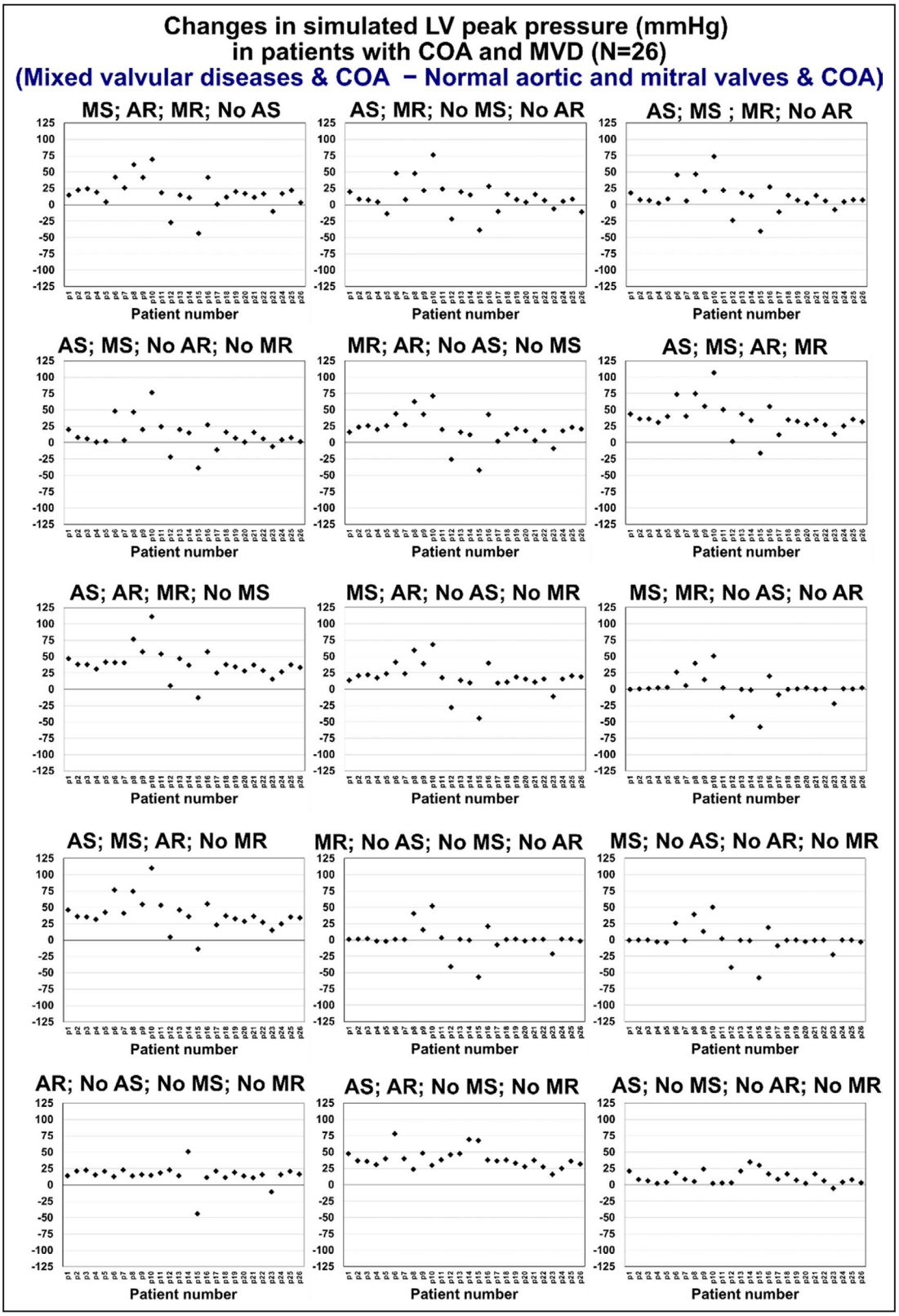

Figure 11. Differences in the simulated LV peak pressure between mixed valvular disease and COA, and normal aortic and mitral valves and COA, in individual patients (N=26).
AR indicates aortic regurgitation; AS, aortic stenosis; COA, coarctation of the aorta; LV, left ventricle; MR, mitral regurgitation; MS, mitral stenosis; and MVD, mixed valvular disease.

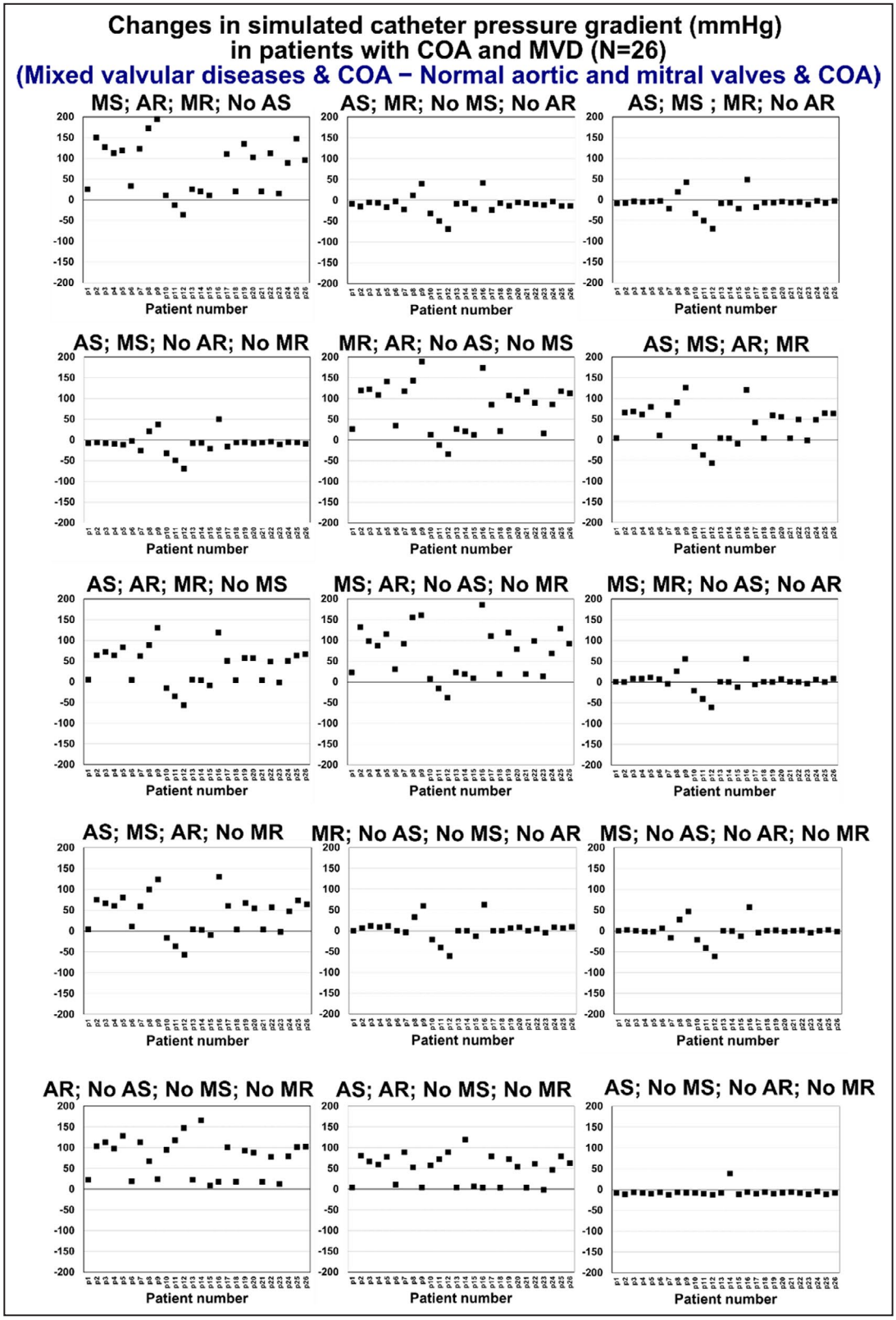

Figure 12. Differences in the simulated catheter pressure gradient between mixed valvular disease and COA, and normal aortic and mitral valves and COA, in individual patients (N=26).
AR indicates aortic regurgitation; AS, aortic stenosis; COA, coarctation of the aorta; MR, mitral regurgitation; MS, mitral stenosis; and MVD, mixed valvular disease.

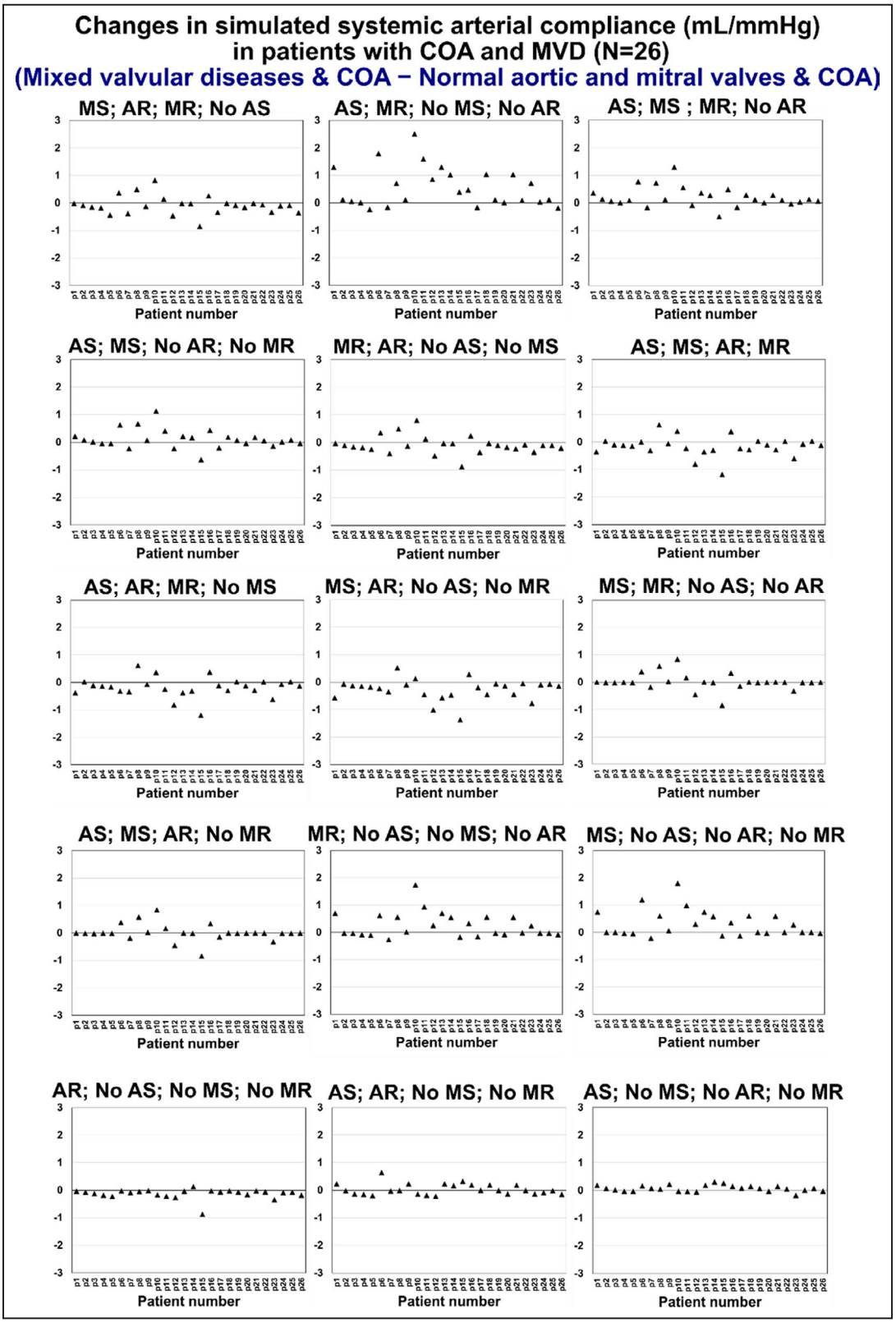

Figure 13. Differences in the simulated systemic arterial compliance between mixed valvular disease and COA, and normal aortic and mitral valves and COA, in individual patients (N=26).
AR indicates aortic regurgitation; AS, aortic stenosis; COA, coarctation of the aorta; MR, mitral regurgitation; MS, mitral stenosis; and MVD, mixed valvular disease.

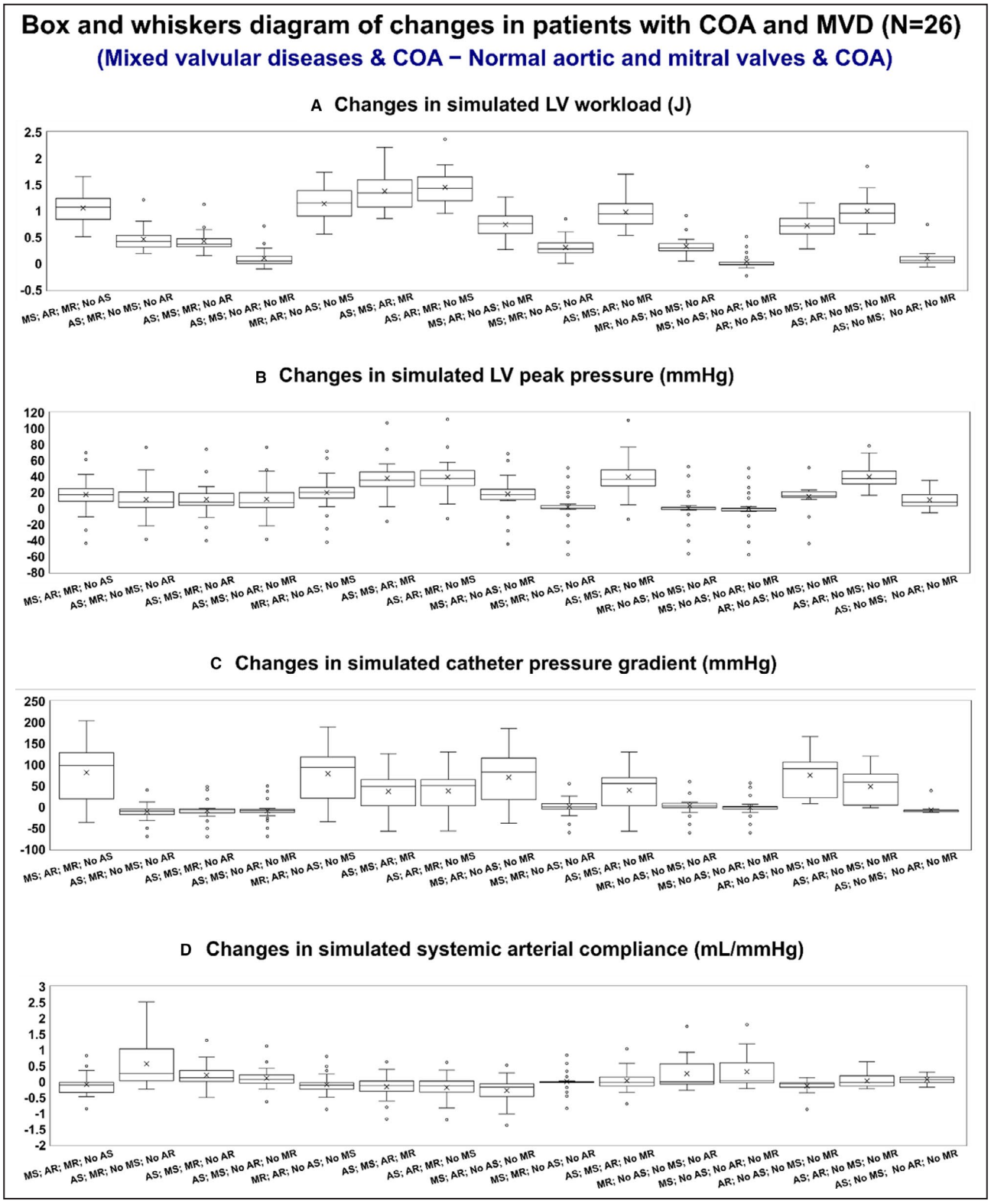

Figure 14. Difference in the simulated hemodynamics parameters between mixed valvular disease and COA, and normal aortic and mitral valves and COA, in all patients (N=26) a using box and whiskers diagram.
A, Simulated LV workload. **B**, Simulated LV peak pressure. **C**, Simulated catheter pressure gradient. **D**, Simulated systemic arterial compliance. AR indicates aortic regurgitation; AS, aortic stenosis; COA, coarctation of the aorta; LV, left ventricle; MR, mitral regurgitation; MS, mitral stenosis; and MVD, mixed valvular disease.

In the current study, to investigate the effect of resolution and to compare LBM and 4D flow MRI velocity fields on identical grids, we downsampled the high-resolution LBM velocity fields by linear interpolation on the 4D flow MRI grid. The downsampling and smoothing procedures are schematically shown in Figure 1.

Statistical Analysis

All results were expressed as mean±SD. Statistical analyses were performed using SigmaStat software (version 3.1;Systat Software, San Jose, CA). Coefficient of determination, R^2, was used to quantify the quality of linear regressions. Statistically significant differences between 2 data sets were assessed using a 2-sample *t* test at a 1% significance level.

RESULTS

Validation: Computational Framework Versus 4D Flow MRI

In this study, we developed a patient-specific, imaged-based computational-mechanics framework that dynamically couples the local hemodynamics with the global circulatory cardiovascular system to investigate the impact of COA and MVDs on both local and global hemodynamics in these patients. The entire computational framework was validated against 4D flow MRI measurements in 5 patients with COA. Figure 2 describes sample cases of voxel-by-voxel Bland-Altman analysis between the velocity fields resulting from the smooth downsampled low-resolution LBM and 4D flow MRI measurements on the entire flow domain at the early systole, the peak systole, as well as the late systole. The simulated velocity fields were in agreement with the velocity fields measured using 4D flow MRI in patients; as examples, average biases (means of differences) were −0.049, −0.059, and 0.0426 m/s, and corresponding average limits of agreement (SD, 1.96) were also ±0.302, ±0.191, and ±0.325 m/s for patients 1, 2, and 3, respectively. Moreover, Figure 3 shows the statistical analyses of the planar velocity differences between velocity field resulting from our computational framework and 4D flow MRI measurements in sample cases at the peak of systole. As this figure shows, the 4D flow MRI velocity field and the downsampled LBM-based velocity fields were compared using Pearson correlation and Bland-Altman analysis. The coefficient of determination (R^2) was used to assess the linearity between the results from 4D flow MRI and our computational framework at these planar sections. The average of coefficients of determination were 0.863, 0.830, 0.526 for patients 1, 2, and 3, respectively. Average lateral section biases (means of differences) were also −0.049, −0.0113, and −0.042 m/s, and the corresponding limits of agreement (SD, 1.96 standard deviation of differences) were ±0.229, ±0.129, and ±0.420 m/s for patients 1, 2, and 3, respectively, which shows agreements between the data resulting from 4D flow MRI and our computational framework. We observed similar agreement (computational results versus 4D flow MRI measurement) in the other patients with COA investigated in this study. It is important to note that 4D flow MRI itself has some limitations, and its measurement involves errors because of low temporal resolution (20 ms highest).[57,67] The differences between the computational results and 4D flow MRI measurements can be partly because of the shortages of 4D flow MRI.

In addition, our developed patient-specific, Doppler-based lumped parameter model calculations were validated against clinical cardiac catheterization data (the instantaneous pressures in the aorta and LV) in patients with complex valvular, ventricular, and vascular diseases with a substantial inter- and intrapatient variability with a wide range of disease (N=49).[49,57] The model has already been validated against in vivo cardiac catheterization in patients with coarctation (N=40),[44,45] and some submodels have been validated against in vivo MRI data (N=57).[68] In addition, some of the submodels of the lumped parameter model have been used and validated previously.[41,49,56,68–76] Moreover, the entire patient-specific computational framework (LBM and lumped parameter model) was validated against clinical Doppler echocardiography previously.[44] Moreover, for all 26 patients investigated in this study, we observed good agreements between the simulated and experimental Doppler echocardiography pressure gradients (mean relative error, 3.9%).

The good agreements between results calculated using our computational framework with the results measured using clinical 4D flow MRI, Doppler echocardiography, and cardiac catheterization allows us to accept our computational results with confidence to investigate the flow features.

Clinical Measure of Hemodynamics: Doppler Echocardiography and Catheter Pressure Gradients

Currently, clinical assessment of COA for management and intervention decisions are achieved based on the symptoms and hemodynamics metrics focused only on COA. A hemodynamically significant COA is often defined as a catheter pressure gradient or Doppler pressure gradient of 20 mmHg across the COA. A COA pressure gradient >20 mmHg warns of major COA and secures interventional/surgical repair. Our data revealed that MVDs and COA have mechanical interactions with one another, alter the pressure gradient across the COA, and lead to overestimating or underestimating the disease (Figures 5, 7, 9, 12, and 14).

As examples, Doppler and catheter pressure gradients were exacerbated significantly in the following cases: COA coexisting with MS, AR, and MR; COA coexisting alongside MR and AR; COA coexisting with MS and AR, and COA coexisting with AR (Figures 5, 7, 9, 12, and 14). This is important because wall expansion, compression, and collapse are caused by high pressure drops in the COA. Moreover, the pressure drops introduced by the presence of the COA and MVDs must be compensated for by the LV, and this in turn can lead to heart failure. Both Doppler and catheter measures documented a transcoarctation pressure gradient in patients with COA and MVDs confirmed the following findings (Figures 5, 7, 9, 12, and 14):

1. The presence of AS alone does not increase the pressure gradient across the COA in patients with COA and MVDs (eg, patient 2: COA with AS alone: 98.60 mmHg [maximum, Doppler echocardiography], 59 mmHg [maximum, catheter]; COA with normal valves: 110 mmHg [maximum, Doppler echocardiography], 78.7 mmHg [maximum, catheter]; Figure 7).
2. COA pressure gradient elevated in the presence of MR alone (eg, patient 2: COA with MR alone: 122.4 mmHg [maximum, Doppler echocardiography], 85.2 mmHg [maximum, catheter]; COA with normal valves: 110 mmHg [max, Doppler echocardiography], 78.7 mmHg [maximum, catheter]; Figure 7).
3. Pressure gradient across the COA drastically increased in the presence of AR alone (eg, patient 2: COA with AR alone: 300.76 mmHg [maximum, Doppler echocardiography], 182.17 mmHg [maximum, catheter]; COA with normal valves: 110 mmHg [maximum, Doppler echocardiography], 78.7 mmHg [maximum, catheter]; Figure 7).
4. The individual COA status remained unchanged in patients with MS alone (eg, patient 2: COA with MS alone: 115 mmHg [Doppler echocardiography], 78.8 mmHg [maximum, catheter]; COA with normal valves: 110 mmHg [Doppler echocardiography], 78.7 mmHg [maximum, catheter]; Figure 7).

We observed similar pressure gradient characteristics in the other patients with COA and MVDs investigated in this study.

Simulated Global and Local Hemodynamics

Global Hemodynamics (Cardiac Function)

The LV workload is an effective metric of the LV function and its clinical state and is calculated as the area encompassed by the LV pressure–volume loop. Our results revealed that LV function parameters (eg, LV pressure and workload) are dramatically different in patients with MVDs. Figures 5, 7, and 9 show examples of LV pressure and workload in 3 patients with COA and MVDs. Our data showed that the LV workload in all COA patients with MVDs was universally increased because of the presence of AS alone, AR alone, MR alone, and when they coexist (Figures 5, 7, 9, 10, 11, and 14). MS alone does not have a remarkable impact on LV workload in these patients. As examples, LV workload and LV pressure in patient 1 are as follows (Figure 5): COA with normal valves: LV workload, 1.0617 J and LV peak pressure, 122.51 mmHg; COA with only AS: LV workload, 1.225 J and LV peak pressure, 143.43 mmHg; COA with only AR: LV workload, 1.6512 J and LV peak pressure, 136.74 mmHg; COA with only MR: LV workload, 1.3599 J and LV peak pressure, 123.48 mmHg; COA with only MS: LV workload, 1.0472 J and LV peak pressure, 122.07 mmHg. We observed similar cardiac function characteristics in the other patients with COA and MVDs.

Local Hemodynamics (Aortic Dynamics)

The presence of the COA itself largely modified the flow dynamics; the disturbed flow resulting from COA detached from the walls and developed into a high-speed eccentric jet. Our data described that the velocity downstream of the COA in all patients with AR alone was drastically increased (Figures 4, 6, and 8). This situation got worse when COA and AR coexisted with MR. As an example, maximum velocities downstream of the COA in patient 2 (Figure 6) are as follows: COA with normal valves: 5.27 m/s, COA with only AR: 8.8 m/s, COA with AR and MR: 9.36 m/s. AR and MR, when coexistent with COA, substantially alter the velocity magnitude downstream of the COA, further encouraging turbulent flow downstream of COA, and may lead to significant progression of the disease at the COA region (Figures 4, 6, and 8). We observed similar characteristics in the other patients with COA and MVDs investigated in this study.

Such flow alterations contributed to elevated wall shear stress mainly at the neck of the COA as well as distal to the COA. Wall shear stress, as a force induced by blood flow, has a major impact on regulating endothelial function and is a predeterminant biomarker of disease progression. In this study, the total shear stress exerted on the aorta wall was evaluated using time-averaged wall shear stress (TAWSS). Our data explained that MVDs impacted TAWSS at the COA region and can further increase the TAWSS (eg, COA coexists with AR alone, COA coexists with MR alone, COA coexists with AR and MR) (Figures 4, 6, and 8) or improve the TAWSS (eg, COA coexists with AS alone) (Figures 4, 6, and 8) at the COA region. Local perturbation in shear stress exposes endothelial cells to high shear stress, which affects vessel distensibility and

compliance and potentially leads to vascular diseases. Although high wall shear stress may act as a deterrent against formation of atherosclerosis, very high wall shear stress can trigger endothelial cells to express a transcriptional profile that ultimately leads to arterial remodeling, rupture, and dissection.

In addition, systemic arterial compliance (stroke volume/pulse pressure) was obtained as an index of arterial hemodynamics. Patients with COA usually have upper extremity hypertension and are characterized by reduced systemic arterial compliance. Our results suggest that any combination of MVDs along with COA substantially alters the systemic arterial compliance magnitudes (Figures 13 and 14).

DISCUSSION

MVDs, which are classified as various combinations of different aortic and mitral valvular pathologies such as AS, AR, bicuspid aortic valve, MR, and MS, are often present in conjunction with COA. We sought to find out if in patients with COA and MVDs the interactions between MVDs and COA have dramatic impacts on both the local and global hemodynamics. It is important to note that in current clinical practice, proper treatment is difficult to administer when COA and MVDs are present. Treatment is often performed in a multiple-stage approach, because higher morbidity rates have been recorded if several pathologies are repaired simultaneously.[22,32,36] It is often unclear what the effects of each pathology are on the cardiovascular system and which pathology is more life threatening. Furthermore, timing of intervention is crucial, because the overload on the LV because of COA and MVDs is likely to lead to LV dysfunction, cardiac failure, and death if not treated promptly.[22,28,77] To date, there are no standardized guidelines, and the ideal treatment methods are often unclear for individuals suffering from COA and MVDs.[34,37] Hemodynamic significance of MVDs and COA must be analyzed carefully to establish proper treatment methods, because an individualized treatment approach is crucial for the optimal recovery of each patient.[40,41] In the present work, there are several findings that should be individually discussed.

Doppler Echocardiography COA Pressure Gradient Is a Poor Indicator of COA Severity When Coexisting With MVDs

Our results demonstrate that in patients who suffered from COA and MVDs (one or a combination of AS, AR, MS, and MR):

1. The presence of AS alone or MS had no major effects on the pressure gradients across the COA measured by Doppler echocardiography. In these patients, the pressure gradient was because of COA itself.
2. Moreover, the COA pressure gradient was nonremarkably elevated in the presence of MR.
3. In contrast, the presence of AR had major effects on the COA pressure gradients; AR interacted with COA and amplified the COA pressure gradients measured by Doppler echocardiography. This is crucial because the high-pressure loss because of COA can be exacerbated by AR, speeding up the collapse of the aorta wall.[8,78–82]

As one example, in the case of COA patient 1 with actual status of severe AS, mild–moderate AR, and mild–moderate MR, the Doppler echocardiography COA pressure gradients (47.3 mmHg [maximum] and 21.50 mmHg [mean]) were almost as if this patient had normal valves (39.8 mmHg [maximum] and 19.09 mmHg [mean]) (Figure 5). This is extremely critical for the following 2 reasons:

1. In the case of COA coexisting with AS alone in this patient (no AR, MR, or MS), Doppler echocardiography COA pressure gradients dropped from 47.3 to 30.7 mmHg (maximum) and from 21.50 to 12.04 mmHg (mean). This shows that the COA pressure gradient may be masked and underestimated in the presence of AS.
2. In the case of COA coexisting with AR alone in this patient (no AS, MR, or MS), Doppler echocardiography COA pressure gradients elevated from 47.3 to 75.2 mmHg (maximum) and from 21.50 to 30.50 mmHg (mean). This reveals that the COA pressure gradient may be overestimated in presence of AR alone.

Catheter Pressure Gradient Fails to Reflect the Effect of MVDs on the Clinical Assessment of COA Hemodynamics

The gold standard for diagnosis and grading of COA is the measurement of the pressure gradient across the site of coarctation by cardiac catheterization.[83] Because precise positioning of the probe in the vena contracta is difficult, probes are typically placed 1 to 2 cm distal to the coarctation, where velocity is reduced and the flow is influenced by the pressure recovery phenomenon, decreasing the accuracy of the measurement.[73,84] In addition to the invasive nature of the procedure that hinders follow-up, and sedation, which is frequently required, it can reduce cardiac activity and lead to an underestimation of the pressure gradient.[85] For patients with COA who also suffer from AS, MS, MR, or a combination, we did not observe major effects because these valvular diseases on the catheter pressure gradient and the measured COA gradient were produced by COA itself (similar to Doppler echocardiography pressure gradients). In contrast, similar to

observations about Doppler echocardiography pressure gradients, the coexistence of AR with COA greatly amplified the catheter COA pressure gradient, leading to an overestimation of the severity of coarctation. Furthermore, catheter (and Doppler) COA pressure gradients are highly influenced by the flow rate, and they are nonlinearly reduced when the flow rate is decreased. The relief of the pressure gradient through COA does not correlate with the relief of symptoms or functional improvements.[84]

MVDs Exacerbated the COA Hemodynamics (Local)

The jets emerging from the COA orifice substantially alter the vortical structure in the aorta, creating disturbed flow, leading to high shear stress mainly downstream of the COA.[8,72,86] Our results demonstrate that MVD interacts with COA fluid dynamics, amplifies irregular flow patterns, and consequently increase TAWSS, especially downstream of COA. In patients with COA who also suffered from AS, MS, or a combination, the presence of these valvular diseases had modest effects on the COA. However, the presence of AR and/or MR, compared with the other valvular diseases (AS and MS), had major impact on the COA hemodynamics as they interacted with COA, and through increasing TAWSS, they may contribute to speeding up the progression of the COA more than other valvular diseases do. These progressions may include endothelial dysfunction, dedifferentiation of the arterial smooth muscle, and medial thickening, all of which can lead to major aortic wall complications such as aortic aneurysm, rupture, and dissection at the COA region.

MVDs Exacerbated the Left Ventricular Function and Hemodynamics (Global)

Our results reveal that COA and some components of MVDs increase the burden on the LV (eg, AS alone, AR alone, MR alone, and when they coexist). Compared with the other valvular diseases, the presence of AR and/or MR, when coexistent with COA, elevates the heart workload significantly because of the increased stroke volume, causing LV volume overload. Therefore, uncorrected COA along with AR and/or MR cause an overloaded LV, resulting in faster deterioration or failure of the LV. To plan interventions as well as their sequence, our findings suggest that not only the severity of the COA and MVDs should be considered, but the breakdown of the effects of each disease constituent on the global function of the heart should also be considered. It is crucial to identify patients in whom AR and/or MR coexists with COA; in these patients, the increased risk of a double procedure may be justified, because correcting one pathology at a time has limited use in reducing myocardial strain and causes persistent increased LV mass and hypertrophy.

Limitations

We developed a computational fluid dynamics framework using a 3D LBM (large eddy simulation, Smagorinsky subgrid scale model) and lumped parameter model to simulate both the local and global hemodynamics in patients with MVDs and COA. One limitation of our simulations is lack of modeling of the aortic and mitral valves. A diseased aortic valve (eg, bicuspid aortic valve or aortic stenosis) creates complex blood flow patterns in the thoracic aorta that influence the local hemodynamics in the coarctation region.[72,87,88] However, the good agreements between results calculated using our computational framework with the results measured using clinical 4D flow MRI, Doppler echocardiography, and cardiac catheterization, which include moving aortic and mitral valves, show that this limitation does not significantly modify the conclusions of this study. Please note that considering moving aortic and mitral valve leaflets as well as modeling the LV are computationally expensive and complicated. Future numerical studies should consider the interactions between the fluid and structure and investigate the effect of dynamical opening and closing of the aortic valve leaflets on the vortex dynamics in the aorta.

ARTICLE INFORMATION

Received May 29, 2021; accepted October 11, 2021.

Affiliations

Department of Mechanical Engineering, McMaster University, Hamilton, Ontario, Canada (R.S., B.T., S.K., Z.K.); Stephenson Cardiac Imaging Centre, Libin Cardiovascular Institute of Alberta, Calgary, Alberta, Canada (J.G.); Department of Radiology (J.G.) and Department of Cardiac Sciences (J.G.), University of Calgary, Calgary, Alberta, Canada; Alberta Children's Hospital Research Institute, Calgary, Alberta, Canada (J.G.); Division of Cardiology, Department of Medicine (J.G.); School of Biomedical Engineering (Z.K.) and School of Computational Science and Engineering (Z.K.), McMaster University, Hamilton, Ontario, Canada; and The Thrombosis & Atherosclerosis Research Institute, McMaster University, Hamilton, Ontario, Canada (Z.K.).

Acknowledgments

The authors acknowledge Compute Canada, the Shared Hierarchical Academic Research Computing Network (www.sharcnet.ca), which provided the computational resources for this study. The authors are thankful for the great comments of 2 anonymous reviewers that helped us to improve the quality of this article.

Author contributions: R.S.: Computational modeling, image processing, data collection and analysis, interpretation of data, and writing the article. B.T. and S.K.: Data collection and analysis, and writing the article; J.Garcia and J.Ganame: Clinical data collection, analysis and interpretation of data. Z.K.-M.: Conception and design, lumped parameter algorithm development, data analysis, interpretation of data, writing the article, critical revision, final approval of the article, and supervised the research. All authors read and approved the final article.

Sources of Funding

This work was supported by Natural Sciences and Engineering Research Council Discovery Grant (RGPIN-2017-05349, RGPIN-2020-04549, and DGECR-2020-00204), and University of Calgary (URGC SEM 105434). The Natural Sciences and Engineering Research Council (https://www.nserc-crsng.gc.ca/index_eng.asp), as the funders, had no role in study design, data collection and analysis, decision to publish, or preparation of the article.

Disclosures

None.

REFERENCES

1. Sinning C, Zengin E, Kozlik-Feldmann R, Blankenberg S, Rickers C, von Kodolitsch Y, Girdauskas E. Bicuspid aortic valve and aortic coarctation in congenital heart disease—important aspects for treatment with focus on aortic vasculopathy. *Cardiovasc Diagn Therapy*. 2018;8:780. doi: 10.21037/cdt.2018.09.20
2. Ma L, Gu Q, Ni B, Sun H, Zhen X, Zhang S, Shao Y. Simultaneously surgical management of adult complex coarctation of aorta concomitant with intracardiac abnormality. *J Thorac Dis*. 2018;10:5842. doi: 10.21037/jtd.2018.09.137
3. Endorsed by the Association for European Paediatric Cardiology, Authors/Task Force Members, Baumgartner H, Bonhoeffer P, De Groot NM, de Haan F, Deanfield JE, Galie N, Gatzoulis MA, Gohlke-Baerwolf C, et al. ESC guidelines for the management of grown-up congenital heart disease (new version 2010) the task force on the management of grown-up congenital heart disease of the European Society of Cardiology (ESC). *Eur Heart J*. 2010;31:2915–2957. doi: 10.1093/eurheartj/ehq249
4. Roos-Hesselink J, Schölzel B, Heijdra R, Spitaels S, Meijboom F, Boersma E, Bogers A, Simoons M. Aortic valve and aortic arch pathology after coarctation repair. *Heart*. 2003;89:1074–1077. doi: 10.1136/heart.89.9.1074
5. Mazzanti L, Prandstraller D, Tassinari D, Rubino I, Santucci S, Picchio F, Forabosco A, Cacciari E. Heart disease in turner's syndrome. *Helvetica Paediatrica Acta*. 1988;43:25–31.
6. Brickner ME, Hillis LD, Lange RA. Congenital heart disease in adults. *N Engl J Med*. 2000;342:256–263. doi: 10.1056/NEJM200001273420407
7. Braverman AC, Güven H, Beardslee MA, Makan M, Kates AM, Moon MR. The bicuspid aortic valve. *Curr Probl Cardiol*. 2005;30:470–522. doi: 10.1016/j.cpcardiol.2005.06.002
8. Keshavarz-Motamed Z, Garcia J, Kadem L. Fluid dynamics of coarctation of the aorta and effect of bicuspid aortic valve. *PLoS One*. 2013;8:e72394. doi: 10.1371/journal.pone.0072394
9. Smith D, Matthews M. Aortic valvular stenosis with coarctation of the aorta: with special reference to the development of aortic stenosis upon congenital bicuspid valves. *Br Heart J*. 1955;17:198. doi: 10.1136/hrt.17.2.198
10. Simon AB, Zloto AE. Coarctation of the aorta: longitudinal assessment of operated patients. *Circulation*. 1974;50:456–464. doi: 10.1161/01.CIR.50.3.456
11. Liberthson RR, Pennington DG, Jacobs ML, Daggett WM. Coarctation of the aorta: review of 234 patients and clarification of management problems. *Am J Cardiol*. 1979;43:835–840. doi: 10.1016/0002-9149(79)90086-9
12. Koller M, Rothlin M, Senning Å. Coarctation of the aorta: review of 362 operated patients. Long-term follow-up and assessment of prognostic variables. *Eur Heart J*. 1987;8:670–679. doi: 10.1093/eurheartj/8.7.670
13. Jost CHA, Schaff HV, Connolly HM, Danielson GK, Dearani JA, Puga FJ, Warnes CA. Spectrum of reoperations after repair of aortic coarctation: importance of an individualized approach because of coexistent cardiovascular disease. *Mayo Clin Proc*. 2002;77:646–653. doi: 10.4065/77.7.646
14. Hamdan MA. Coarctation of the aorta: a comprehensive review. *Prevalence*. 2006;50:30.
15. Popescu BA, Jurcut R, Serban M, Parascan L, Ginghina C. Shone's syndrome diagnosed with echocardiography and confirmed at pathology. *Eur J Echocardiogr*. 2008;9:865–867. doi: 10.1093/ejechocard/jen200
16. Ganju NK, Kandoria A, Thakur S, Ganju SA. A constellation of cardiac anomalies: beyond shone's complex. *Heart Views*. 2016;17:23. doi: 10.4103/1995-705X.182643
17. Celano V, Pieroni DR, Morera JA, Roland J-M, Gingell R. Two-dimensional echocardiographic examination of mitral valve abnormalities associated with coarctation of the aorta. *Circulation*. 1984;69:924–932. doi: 10.1161/01.CIR.69.5.924
18. Rosenquist GC. Congenital mitral valve disease associated with coarctation of the aorta: a spectrum that includes parachute deformity of the mitral valve. *Circulation*. 1974;49:985–993. doi: 10.1161/01.CIR.49.5.985
19. Omran A, Arifi AA, Mohamed A. Echocardiography in mitral stenosis. *J Saudi Heart Assoc*. 2011;23:51–58. doi: 10.1016/j.jsha.2010.07.007
20. Ludman P, Yacoub M, Dancy M. Mitral valve prolapse and occult aortic coarctation. *Postgrad Med J*. 1990;66:834–837. doi: 10.1136/pgmj.66.780.834
21. Easthope R, Tawes RL Jr, Bonham-Carter R, Aberdeen E, Waterston D. Congenital mitral valve disease associated with coarctation of the aorta: a report of 39 cases. *Am Heart J*. 1969;77:743–754. doi: 10.1016/0002-8703(69)90408-6
22. Cartier R, Ugolini P, Paquet E. Severe aortic insufficiency associated with left ventricular dysfunction and aortic coarctation. *Can J Surg*. 2002;45:213.
23. Becker AE, Becker MJ, Edwards JE. Anomalies associated with coarctation of aorta particular reference to infancy. *Circulation*. 1970;41:1067–1075. doi: 10.1161/01.CIR.41.6.1067
24. Baumgartner H, Hung J, Bermejo J, Chambers JB, Evangelista A, Griffin BP, Iung B, Otto CM, Pellikka PA, Quiñones M. Echocardiographic assessment of valve stenosis: EAE/ASE recommendations for clinical practice. *J Am Soc Echocardiogr*. 2009;22:1–23. doi: 10.1016/j.echo.2008.11.029
25. Wood WC, Wood JC, Lower RR, Bosher LH Jr, McCue CM. Associated coarctation of the aorta and mitral valve disease: nine cases with surgical correction of both lesions in three. *J Pediatr*. 1975;87:217–220. doi: 10.1016/S0022-3476(75)80582-8
26. Warnes C. Bicuspid aortic valve and coarctation: two villains part of a diffuse problem. *Heart*. 2003;89:965–966. doi: 10.1136/heart.89.9.965
27. Mangoni AA, Koelling TM, Meyer GS, Akins CW, Fifer MA. Outcome following mitral valve replacement in patients with mitral stenosis and moderately reduced left ventricular ejection fraction. *Eur J Cardiothorac Surg*. 2002;22:90–94. doi: 10.1016/S1010-7940(02)00218-X
28. Jashari H, Rydberg A, Ibrahimi P, Bajraktari G, Henein MY. Left ventricular response to pressure afterload in children: aortic stenosis and coarctation: a systematic review of the current evidence. *Int J Cardiol*. 2015;178:203–209. doi: 10.1016/j.ijcard.2014.10.089
29. Enriquez-Sarano M, Avierinos J-F, Messika-Zeitoun D, Detaint D, Capps M, Nkomo V, Scott C, Schaff HV, Tajik AJ. Quantitative determinants of the outcome of asymptomatic mitral regurgitation. *N Engl J Med*. 2005;352:875–883. doi: 10.1056/NEJMoa041451
30. Bekeredjian R, Grayburn PA. Valvular heart disease: aortic regurgitation. *Circulation*. 2005;112:125–134. doi: 10.1161/CIRCULATIONAHA.104.488825
31. Terzaki AK, Leachman RD, Ali MK, Hallman GL, Cooley DA. Congenital mitral incompetence and coarctation of aorta: report of two cases treated surgically. *Thorax*. 1972;27:729–737. doi: 10.1136/thx.27.6.729
32. Brown JW, Dunn JM, Brymer JF, Kirsh MM. Simultaneous treatment of aortic stenosis and coarctation by left thoracotomy with apical aortic conduit. *Ann Thorac Surg*. 1978;25:364–367. doi: 10.1016/S0003-4975(10)63559-X
33. Brauner RA, Laks H, Drinkwater DC Jr, Scholl F, McCaffery S. Multiple left heart obstructions (Shone's anomaly) with mitral valve involvement: long-term surgical outcome. *Ann Thorac Surgery*. 1997;64:721–729. doi: 10.1016/S0003-4975(97)00632-2
34. Velinović M, Karan R, Kovačević-Kostić N, Obrenović-Kirćanski B, Stojimirov M, Milićević V, Nikolić D, Milić D. Aortic coarctation and associated cardiac lesions: optimal therapeutic approach: report of 2 cases. *Vojnosanit Pregl*. 2019;76:1197–1202. doi: 10.2298/VSP171018027V
35. Teixeira AM, Reis-Santos K, Anjos R. Hybrid approach to severe coarctation and aortic regurgitation. *Cardiol Young*. 2005;15:525. doi: 10.1017/S1047951105001435
36. Mulay AV, Ashraf S, Watterson KG. Two-stage repair of adult coarctation of the aorta with congenital valvular lesions. *Annals Thorac Surg*. 1997;64:1309–1311. doi: 10.1016/S0003-4975(97)00814-X
37. Koletsis E, Ekonomidis S, Panagopoulos N, Tsaousis G, Crockett J, Panagiotou M. Two stage hybrid approach for complex aortic coarctation repair. *J Cardiothorac Surg*. 2009;4:10. doi: 10.1186/1749-8090-4-10
38. Bolling SF, Iannettoni MD, Dick M II, Rosenthal A, Bove EL. Shone's anomaly: operative results and late outcome. *Ann Thorac Surg*. 1990;49:887–893. doi: 10.1016/0003-4975(90)90861-Y
39. Zhang H, Zhu K, Yang S, Zhai J, Zhou T, Sun X, Wang C. Bicuspid aortic valve with critical coarctation of the aorta: single-or two-stage operation? *J Thorac Dis*. 2018;10:4353. doi: 10.21037/jtd.2018.06.112
40. Kumar S, Goud A, Versha F, Mukherjee A, Pai R. Coarctation of aorta in an adult with severe aortic stenosis: deciding on the optimal approach. *J Am Coll Cardiol*. 2018;71:A2160. doi: 10.1016/S0735-1097(18)32701-3
41. Keshavarz-Motamed Z, Garcia J, Pibarot P, Larose E, Kadem L. Modeling the impact of concomitant aortic stenosis and coarctation of the aorta on left ventricular workload. *J Biomech*. 2011;44:2817–2825. doi: 10.1016/j.jbiomech.2011.08.001

42. Richter Y, Edelman ER, Cardiology is flow. *Circulation*. 2006;113:2679–2682. doi: 10.1161/CIRCULATIONAHA.106.632687
43. Anvari S, Nambiar S, Pang J, Maftoon N. Computational models and simulations of cancer metastasis. *Arch Comput Methods Eng*. 2021;1–23. doi: 10.1007/s11831-021-09554-1
44. Sadeghi R, Khodaei S, Ganame J, Keshavarz-Motamed Z. Towards non-invasive computational-mechanics and imaging-based diagnostic framework for personalized cardiology for coarctation. *Sci Rep*. 2020;10:1–19. doi: 10.1038/s41598-020-65576-y
45. Keshavarz-Motamed Z, Rikhtegar Nezami F, Partida RA, Nakamura K, Staziaki PV, Ben-Assa E, Ghoshhajra B, Bhatt AB, Edelman ER. Elimination of transcoarctation pressure gradients has no impact on left ventricular function or aortic shear stress after intervention in patients with mild coarctation. *JACC Cardiovasc Interv*. 2016;9:1953–1965. doi: 10.1016/j.jcin.2016.06.054
46. Karaosmanoglu AD, Khawaja RDA, Onur MR, Kalra MK. CT and MRI of aortic coarctation: pre-and postsurgical findings. *Am J Roentgenol*. 2015;204:W224–W233. doi: 10.2214/AJR.14.12529
47. Garber L, Khodaei S, Keshavarz-Motamed Z. The critical role of lumped parameter models in patient-specific cardiovascular simulations. *Arch Computat Methods Eng*. 2021:1–24. doi: 10.1007/s11831-021-09685-5
48. Keshavarz Motamed P, Maftoon N. A systematic approach for developing mechanistic models for realistic simulation of cancer cell motion and deformation. *Sci Rep*. 2021;11:21545. doi: 10.1038/s41598-021-00905-3
49. Keshavarz-Motamed Z. A diagnostic, monitoring, and predictive tool for patients with complex valvular, vascular and ventricular diseases. *Sci Rep*. 2020;10:1–19. doi: 10.1038/s41598-020-63728-8
50. Mittal R, Simmons S, Udaykumar H. Application of large-eddy simulation to the study of pulsatile flow in a modeled arterial stenosis. *J Biomech Eng*. 2001;123:325–332. doi: 10.1115/1.1385840
51. Skordos P. Initial and boundary conditions for the lattice Boltzmann method. *Phys Rev E*. 1993;48:4823. doi: 10.1103/PhysRevE.48.4823
52. Heuveline V, Krause MJ, Latt J. Towards a hybrid parallelization of lattice boltzmann methods. *Comput Math Appl*. 2009;58:1071–1080. doi: 10.1016/j.camwa.2009.04.001
53. Henn T, Heuveline V, Krause MJ, Ritterbusch S. Aortic coarctation simulation based on the lattice Boltzmann method: benchmark results. *Int Workshop Stat Atlases Comput Models Heart*. 2012:34-43.
54. Mirzaee H, Henn T, Krause MJ, Goubergrits L, Schumann C, Neugebauer M, Kuehne T, Preusser T, Hennemuth A. MRI-based computational hemodynamics in patients with aortic coarctation using the lattice boltzmann methods: clinical validation study. *J Magn Reson Imaging*. 2017;45:139–146. doi: 10.1002/jmri.25366
55. Jin S, Oshinski J, Giddens DP. Effects of wall motion and compliance on flow patterns in the ascending aorta. *J Biomech Eng*. 2003;125:347–354. doi: 10.1115/1.1574332
56. Keshavarz-Motamed Z, Edelman ER, Motamed PK, Garcia J, Dahdah N, Kadem L. The role of aortic compliance in determination of coarctation severity: lumped parameter modeling, in vitro study and clinical evaluation. *J Biomech*. 2015;48:4229–4237. doi: 10.1016/j.jbiomech.2015.10.017
57. Baiocchi M, Barsoum S, Khodaei S, de la Torre Hernandez JM, Valentino SE, Dunford EC, MacDonald MJ, Keshavarz-Motamed Z. Effects of choice of medical imaging modalities on a non-invasive diagnostic and monitoring computational framework for patients with complex valvular, vascular, and ventricular diseases who undergo transcatheter aortic valve replacement. *Front Bioeng Biotechnol*. 2021;389. doi: 10.3389/fbioe.2021.643453
58. Bouzidi MH, Firdaouss M, Lallemand P. Momentum transfer of a boltzmann-lattice fluid with boundaries. *Phys Fluids*. 2001;13:3452–3459. doi: 10.1063/1.1399290
59. Nathen P, Gaudlitz D, Krause M, Kratzke J. An extension of the lattice boltzmann method for simulating turbulent flows around rotating geometries of arbitrary shape. *21st AIAA Comput Fluid Dyn Conf. Am Inst Aeronaut Astronaut*. 2013;2753.
60. Stankovic Z, Allen BD, Garcia J, Jarvis KB, Markl M. 4D flow imaging with MRI. *Cardiovasc Diagn Ther*. 2014;4:173. doi: 10.3978/j.issn.2223-3652.2014.01.02
61. Van Ooij P, Garcia J, Potters WV, Malaisrie SC, Collins JD, Carr JC, Markl M, Barker AJ. Age-related changes in aortic 3D blood flow velocities and wall shear stress: implications for the identification of altered hemodynamics in patients with aortic valve disease. *J Magn Reson Imaging*. 2016;43:1239–1249. doi: 10.1002/jmri.25081
62. Marlevi D, Ruijsink B, Balmus M, Dillon-Murphy D, Fovargue D, Pushparajah K, Bertoglio C, Colarieti-Tosti M, Larsson M, Lamata P, et al. Estimation of cardiovascular relative pressure using virtual work-energy. *Sci Rep*. 2019;9:1–16. doi: 10.1038/s41598-018-37714-0
63. Hassanabad AF, Burns F, Bristow MS, Lydell C, Howarth AG, Heydari B, Gao X, Fedak PW, White JA, Garcia J. Pressure drop mapping using 4D flow MRI in patients with bicuspid aortic valve disease: a novel marker of valvular obstruction. *Magn Reson Imaging*. 2020;65:175–182. doi: 10.1016/j.mri.2019.11.011
64. Garcia J, Barker AJ, Markl M. The role of imaging of flow patterns by 4D flow MRI in aortic stenosis. *JACC Cardiovasc Imaging*. 2019;12:252–266. doi: 10.1016/j.jcmg.2018.10.034
65. Garcia D. A fast all-in-one method for automated post-processing of piv data. *Exp Fluids*. 2011;50:1247–1259. doi: 10.1007/s00348-010-0985-y
66. Garcia D. Robust smoothing of gridded data in one and higher dimensions with missing values. *Comput Stat Data Anal*. 2010;54:1167–1178. doi: 10.1016/j.csda.2009.09.020
67. Shen J, Faruqi AH, Jiang Y, Maftoon N. Mathematical reconstruction of patient-specific vascular networks based on clinical images and global optimization. *IEEE Access*. 2021;9:20648–20661. doi: 10.1109/ACCESS.2021.3052501
68. Keshavarz-Motamed Z, Garcia J, Gaillard E, Capoulade R, Le Ven F, Cloutier G, Kadem L, Pibarot P. Non-invasive determination of left ventricular workload in patients with aortic stenosis using magnetic resonance imaging and doppler echocardiography. *PLoS One*. 2014;9:e86793. doi: 10.1371/journal.pone.0086793
69. Asaadi M, Mawad W, Djebbari A, Keshavardz-Motamed Z, Dahdah N, Kadem L. On left ventricle stroke work efficiency in children with moderate aortic valve regurgitation or moderate aortic valve stenosis. *Pediatr Cardiol*. 2021;1–9. doi: 10.1007/s00246-021-02690-2
70. Ben-Assa E, Brown J, Keshavarz-Motamed Z, de la Torre Hernandez JM, Leiden B, Olender M, Kallel F, Palacios IF, Inglessis I, Passeri JJ, et al. Ventricular stroke work and vascular impedance refine the characterization of patients with aortic stenosis. *Sci Transl Med*. 2019;11:eaaw0181. doi: 10.1126/scitranslmed.aaw0181
71. Benevento E, Djebbari A, Keshavarz-Motamed Z, Cecere R, Kadem L. Hemodynamic changes following aortic valve bypass: a mathematical approach. *PLoS One*. 2015;10:e0123000. doi: 10.1371/journal.pone.0123000
72. Keshavarz-Motamed Z, Garcia J, Gaillard E, Maftoon N, Di Labbio G, Cloutier G, Kadem L. Effect of coarctation of the aorta and bicuspid aortic valve on flow dynamics and turbulence in the aorta using particle image velocimetry. *Exp Fluids*. 2014;55:1–16. doi: 10.1007/s00348-014-1696-6
73. Keshavarz-Motamed Z, Garcia J, Maftoon N, Bedard E, Chetaille P, Kadem L. A new approach for the evaluation of the severity of coarctation of the aorta using Doppler velocity index and effective orifice area: in vitro validation and clinical implications. *J Biomech*. 2012;45:1239–1245. doi: 10.1016/j.jbiomech.2012.01.039
74. Keshavarz-Motamed Z, Khodaei S, Rikhtegar Nezami F, Amrute JM, Lee SJ, Brown J, Ben-Assa E, Garcia Camarero T, Ruano Calvo J, Sellers S, et al. Mixed valvular disease following transcatheter aortic valve replacement: quantification and systematic differentiation using clinical measurements and image-based patient-specific in silico modeling. *J Am Heart Assoc*. 2020;9:e015063. doi: 10.1161/JAHA.119.015063
75. Khodaei S, Henstock A, Sadeghi R, Sellers S, Blanke P, Leipsic J, Emadi A, Keshavarz-Motamed Z. Personalized intervention cardiology with transcatheter aortic valve replacement made possible with a non-invasive monitoring and diagnostic framework. *Sci Rep*. 2021;11:1–28. doi: 10.1038/s41598-021-85500-2
76. Khodaei S, Sadeghi R, Blanke P, Leipsic J, Emadi A, Keshavarz-Motamed Z. Towards a non-invasive computational diagnostic framework for personalized cardiology of transcatheter aortic valve replacement in interactions with complex valvular, ventricular and vascular disease. *Int J Mech Sci*. 2021;202:106506. doi: 10.1016/j.ijmecsci.2021.106506
77. Spain MG, Smith MD, Grayburn PA, Harlamert EA, Demaria AN, O'Brien M, Kwan OL. Quantitative assessment of mitral regurgitation by Doppler color flow imaging: angiographic and hemodynamic correlations. *J Am Coll Cardiol*. 1989;13:585–590. doi: 10.1016/0735-1097(89)90597-4
78. Wendell DC, Samyn MM, Cava JR, Ellwein LM, Krolikowski MM, Gandy KL, Pelech AN, Shadden SC, LaDisa JF Jr. Including aortic valve morphology in computational fluid dynamics simulations: initial findings and application to aortic coarctation. *Med Eng Phys*. 2013;35:723–735. doi: 10.1016/j.medengphy.2012.07.015

79. Siu SC, Silversides CK. Bicuspid aortic valve disease. *J Am Coll Cardiol*. 2010;55:2789–2800. doi: 10.1016/j.jacc.2009.12.068
80. Hope MD, Meadows AK, Hope TA, Ordovas KG, Reddy GP, Alley MT, Higgins CB. Evaluation of bicuspid aortic valve and aortic coarctation with 4D flow magnetic resonance imaging. *Circulation*. 2008;117:2818–2819. doi: 10.1161/CIRCULATIONAHA.107.760124
81. Davies RR, Kaple RK, Mandapati D, Gallo A, Botta DM Jr, Elefteriades JA, Coady MA. Natural history of ascending aortic aneurysms in the setting of an unreplaced bicuspid aortic valve. *Ann Thorac Surg*. 2007;83:1338–1344. doi: 10.1016/j.athoracsur.2006.10.074
82. Ayad RF, Grayburn PA, Ko JM, Filardo G, Roberts WC. Accuracy of two-dimensional echocardiography in determining aortic valve structure in patients >50 years of age having aortic valve replacement for aortic stenosis. *Am J Cardiol*. 2011;108:1589–1599. doi: 10.1016/j.amjcard.2011.09.006
83. Kim YY, Andrade L, Cook SC. Aortic coarctation. *Cardiol Clin*. 2020;38:337–351. doi: 10.1016/j.ccl.2020.04.003
84. Seifert BL, DesRochers K, Ta M, Giraud G, Zarandi M, Gharib M, Sahn DJ. Accuracy of Doppler methods for estimating peak-to-peak and peak instantaneous gradients across coarctation of the aorta: an in vitro study. *J Am Soc Echocardiogr*. 1999;12:744–753. doi: 10.1016/S0894-7317(99)70025-8
85. Brüning J, Hellmeier F, Yevtushenko P, Kühne T, Goubergrits L. Uncertainty quantification for non-invasive assessment of pressure drop across a coarctation of the aorta using CFD. *Cardiovasc Eng Technol*. 2018;9:582–596. doi: 10.1007/s13239-018-00381-3
86. Keshavarz-Motamed Z, Kadem L. 3D pulsatile flow in a curved tube with coexisting model of aortic stenosis and coarctation of the aorta. *Med Eng Phys*. 2011;33:315–324. doi: 10.1016/j.medengphy.2010.10.017
87. Lavon K, Halevi R, Marom G, Ben Zekry S, Hamdan A, Joachim Schäfers H, Raanani E, Haj-Ali R. Fluid–structure interaction models of bicuspid aortic valves: the effects of nonfused cusp angles. *J Biomech Eng*. 2018;140:031010. doi: 10.1115/1.4038329
88. de Oliveira DM, Abdullah N, Green NC, Espino DM. Biomechanical assessment of bicuspid aortic valve phenotypes: a fluid–structure interaction modelling approach. *Cardiovasc Eng Technol*. 2020;11:431–447. doi: 10.1007/s13239-020-00469-9